Volume 22
Number 43
21 November 2020
Pages 24817–25410

PCCP

Physical Chemistry Chemical Physics

rsc.li/pccp

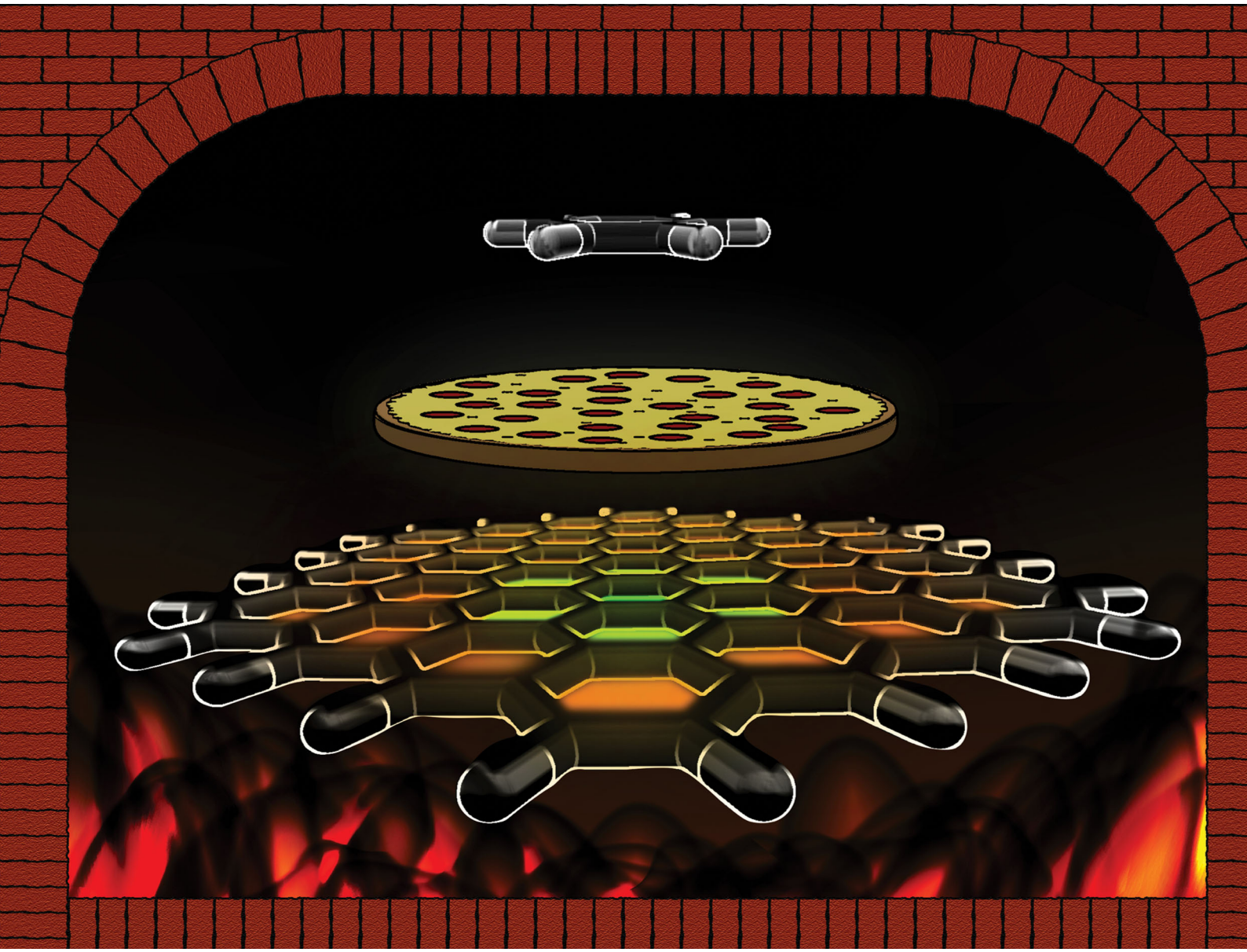

ISSN 1463-9076

ROYAL SOCIETY OF CHEMISTRY

PAPER
Kevin Carter-Fenk and John M. Herbert
Reinterpreting π-stacking

PCCP

ROYAL SOCIETY OF CHEMISTRY

PAPER

View Article Online
View Journal | View Issue

Check for updates

Cite this: *Phys. Chem. Chem. Phys.*, 2020, **22**, 24870

Reinterpreting π-stacking†

Kevin Carter-Fenk and John M. Herbert *

The nature of π–π interactions has long been debated. The term "π-stacking" is considered by some to be a misnomer, in part because overlapping π-electron densities are thought to incur steric repulsion, and the physical origins of the widely-encountered "slip-stacked" motif have variously been attributed to either sterics or electrostatics, in competition with dispersion. Here, we use quantum-mechanical energy decomposition analysis to investigate π–π interactions in supramolecular complexes of polycyclic aromatic hydrocarbons, ranging in size up to realistic models of graphene, and for comparison we perform the same analysis on stacked complexes of polycyclic saturated hydrocarbons, which are cyclohexane-based analogues of graphane. Our results help to explain the short-range structure of liquid hydrocarbons that is inferred from neutron scattering, trends in melting-point data, the interlayer separation of graphene sheets, and finally band gaps and observation of molecular plasmons in graphene nanoribbons. Analysis of intermolecular forces demonstrates that aromatic π–π interactions constitute a unique and fundamentally quantum-mechanical form of non-bonded interaction. Not only do stacked π–π architectures enhance dispersion, but quadrupolar electrostatic interactions that may be repulsive at long range are rendered attractive at the intermolecular distances that characterize π-stacking, as a result of charge penetration effects. The planar geometries of aromatic sp^2 carbon networks lead to attractive interactions that are "served up on a molecular pizza peel", and adoption of slip-stacked geometries minimizes steric (rather than electrostatic) repulsion. The slip-stacked motif therefore emerges not as a defect induced by electrostatic repulsion but rather as a natural outcome of a conformational landscape that is dominated by van der Waals interactions (dispersion plus Pauli repulsion), and is therefore fundamentally quantum-mechanical in its origins. This reinterpretation of the forces responsible for π-stacking has important implications for the manner in which non-bonded interactions are modeled using classical force fields, and for rationalizing the prevalence of the slip-stacked π–π motif in protein crystal structures.

Received 23rd September 2020,
Accepted 12th October 2020

DOI: 10.1039/d0cp05039c

rsc.li/pccp

Published on 13 October 2020. Downloaded on 11/11/2020 5:31:14 PM.

1 Introduction

Is there a special type of dispersion associated with π–π interactions? Some studies suggest that there is, citing the relationship between the π-stacking distance in aromatic π–π systems and the strength of the dispersion interaction.[1] Others point out that aromaticity is not a necessary condition for obtaining augmented dispersion in π-electron systems, and in fact can sometimes lead to additional Pauli (steric) repulsion that diminishes the attractive interaction.[2,3] In view of this, structural rigidity of the interacting moieties may be a more incisive metric for predicting enhanced attraction.[4] Complicating the picture is the fact that aromatic rings often possess large quadrupole moments,[5,6] bringing an electrostatic angle to the problem, and this consideration has fomented a suggestion that the term "π-stacking" should be reconsidered altogether.[7] Arguments based on classical multipole moments, however, seem ill-suited to explain the prevalence of the slip-stacked motif between aromatic side chains in protein crystal structures,[8–10] where the data presumably sample a broad range of electrostatic environments. Nevertheless, quadrupolar electrostatics is a recurring theme in discussion of π–π interactions, and has long been the principle paradigm through which parallel-displaced π-stacking has been rationalized.[9–21] This conventional wisdom persists despite considerable evidence that charge penetration effects, which nullify or at least complicate classical electrostatic arguments, are significant at typical π-stacking distances.[22–29]

Benzene dimer is the archetypal π-stacked system and its conformational preferences are traditionally discussed in terms of several geometric isomers that are depicted in Fig. 1. The cofacial geometry (Fig. 1a) represents canonical π-stacking, although for $(C_6H_6)_2$ in the gas phase this geometry is an energetic saddle point

Department of Chemistry & Biochemistry, The Ohio State University, Columbus, OH, USA. E-mail: herbert@chemistry.ohio-state.edu

† Electronic supplementary information (ESI) available: Additional potential energy surfaces for π-stacked systems, geometries for all systems studied, and range-separation parameters for the LRC-ωPBE functional used for the XSAPT+MBD calculations. See DOI: 10.1039/d0cp05039c

This journal is © the Owner Societies 2020

Published on 13 October 2020. Downloaded on 11/11/2020 5:31:14 PM.

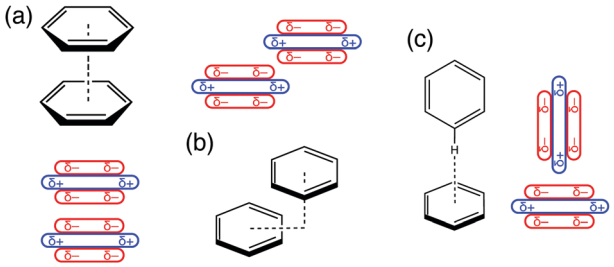

Fig. 1 Geometric motifs in $(C_6H_6)_2$, with an illustration of the quadrupolar electrostatic picture for each: (a) cofacial π-stacked geometry, (b) parallel-offset or slip-stacked geometry, and (c) perpendicular (T-shaped or CH···π) geometry. Reprinted from ref. 29, published by the Royal Society of Chemistry.

along a sliding coordinate leading to the parallel-offset (or slip-stacked) geometry in Fig. 1b.[30] The slip-stacked isomer is a local minimum, and is nearly iso-energetic with the T-shaped isomer depicted in Fig. 1c.[13,30–33] The perfectly perpendicular T-shaped geometry is a saddle point in the gas phase,[32] and tilts by a few degrees along the pendular CH···π coordinate to lower the energy by 0.2 kcal mol^{-1},[32,33] but this will not concern us here. In fact, we will argue that benzene dimer is not representative of π–π interactions in larger polycyclic aromatic hydrocarbons (PAHs), and thus undeserving of its paradigmatic status.

The traditional explanation for the geometry preferences of $(C_6H_6)_2$, as formalized long ago by Hunter and Sanders,[11] is based on a competition between attractive dispersion and repulsive quadrupolar electrostatics. While the Hunter–Sanders model correctly predicts a slip-stacked structure for $(C_6H_6)_2$, in agreement with *ab initio* calculations, it does not explain the fact that $(C_6H_6)\cdots(C_6F_6)$ also exhibits a parallel-offset structure,[34–36] despite quadrupolar electrostatic interactions that are attractive in the cofacial arrangement. Various studies have since suggested that the Hunter–Sanders model exaggerates the role of electrostatics,[3,22–26,32,37–41] however this model remains a widely-discussed paradigm for π–π interactions,[9–21] highlighted in contemporary textbooks.[14,15]

We have recently provided a clear and concise demonstration that the importance of electrostatics in π–π interactions has been misconstrued, and that the Hunter–Sanders model does not simply "overemphasize" electrostatics,[1] but is in fact qualitatively wrong and represents a fundamentally flawed framework for understanding π–π interactions.[29] Rather than being dictated by quadrupolar electrostatics, conformational preferences in systems such as $(C_6H_6)_2$ and $(C_6H_6)\cdots(C_6F_6)$ are instead driven by van der Waals (vdW) interactions, by which we mean a combination of dispersion and Pauli repulsion. The vdW model provides a unified explanation for the emergence of a slip-stacked geometry in both cofacial $(C_6H_6)_2$, where the quadrupolar interaction is repulsive, but also in $(C_6H_6)\cdots(C_6F_6)$, were the polarity of the C–F bonds reverses the sign of the C_6F_6 quadrupole moment, relative to that of C_6H_6.[5,6]

The problem with the classical quadrupole model is that it fail to account for charge penetration at short range.[24,27,29,42] Note that charge penetration is a fundamentally different concept than intermolecular charge transfer.[21] The latter describes a particular form of polarization, whose definition can be quite sensitive to the choice of orbitals and basis set,[43] but which is rather small for the systems considered here. This may be inferred experimentally by the absence of significant vibrational frequency shifts upon complexation, even in systems like $(C_6H_6)\cdots(C_6F_6)$,[6] and also theoretically by the rather small induction energies that are reported in this work. Instead, the term "charge penetration" describes the fact that a low-order multipole expansion may misrepresent the electrostatic interaction energy,

$$E_{\mathrm{elst}} = \iint \frac{\rho_{\mathrm{A}}(\mathbf{r}_1)\rho_{\mathrm{B}}(\mathbf{r}_2)}{\|\mathbf{r}_1 - \mathbf{r}_2\|} \mathrm{d}\mathbf{r}_1 \mathrm{d}\mathbf{r}_2, \quad (1)$$

specifically at short intermolecular distances where the monomer charge densities interpenetrate. Unlike the problematic definition of charge transfer,[43] however, there is no ambiguity in the definition of E_{elst} because $\rho_{\mathrm{A}}(\mathbf{r})$ and $\rho_{\mathrm{B}}(\mathbf{r})$ are isolated monomer densities. Any deviation between eqn (1) and a multipolar approximation is a manifestation of charge penetration.

In benzene dimer, charge penetration effects largely mitigate the electrostatic preference for a cofacial *versus* a slip-stacked arrangement, and the latter emerges as the preferred geometry due to a competition between dispersion and Pauli repulsion, rather than between dispersion and electrostatics.[29] This can be modeled using a simple vdW (repulsion + dispersion) potential that reproduces *ab initio* geometries for benzene dimer, naphthalene dimer, and $(C_6H_6)\cdots(C_6F_6)$.[29] Offset π-stacking can thus be understood without appeal to electrostatics at all! This helps to rationalize the persistence of the offset-stacked motif in the π–π side-chain interactions in proteins, which are revealed by data-mining studies of the protein data bank.[8–10] In view of this new interpretation of π-stacking, it seems pertinent to revisit old questions regarding whether π–π interactions truly constitute a unique form of dispersion.

The concept of π-stacking has elicited controversy, perhaps due to an incomplete definition of the phenomenon. The terminology seems to suggest significant overlap between π-electron clouds of two moieties in a cofacial arrangement. From the standpoint of dispersion, which varies with distance as $\sim\bar{\alpha}/R^6$ where $\bar{\alpha}$ denotes the isotropic polarizability, the cofacial arrangement minimizes interatomic distances and therefore maximizes the attraction due to dispersion. On the other hand, exchange repulsion (*i.e.*, steric or Pauli repulsion) is proportional to the overlap integral S between molecular orbitals and decays as $\sim S^2/R$.[44,45] Any overlap between π clouds is therefore repulsive to some extent. Recent work by Tkatchenko and co-workers has also highlighted the role of charge-density fluctuations in stabilizing nanoscale π–π interactions.[46,47]

Grimme[1] and others[48] have examined stacking of both aromatic and saturated hydrocarbons as a function of size, concluding that for larger acene dimers there is a clear enhancement of the interaction energy in cofacial arrangements, beyond what is seen in perpendicular orientations that are analogous to the T-shaped isomer of $(C_6H_6)_2$. Interaction energies between saturated hydrocarbons exhibit size dependence that is much closer to that of perpendicular acene dimers.[1,48] One goal of the present work is

Published on 13 October 2020. Downloaded on 11/11/2020 5:31:14 PM.

to reexamine these size-dependent trends in view of our new understanding of the role of vdW forces.

The role of electrostatics is more complicated. Grimme's analysis is framed against the backdrop of the Hunter–Sanders model,[1] with its assumption that electrostatic interactions are repulsive in cofacial π-stacked arrangements and that this repulsion drives offset-stacking. In fact, charge penetration effects are significant at typical π-stacking distances, as documented by Sherrill[22–26] and by others.[27,28] In acene dimers, for example, the exact electrostatic interaction energy computed using eqn (1) deviates from the leading-order quadrupolar result by as much as 50% at crystal-packing distances.[27] That said, previous *ab initio* studies of electrostatic effects in π-stacked systems have focused on single-point energy decompositions or on the intermolecular separation coordinate. As we showed previously for $(C_6H_6)_2$,[29] the role of vdW forces in determining the conformational landscape emerges only upon consideration of the potential energy surface for sliding one molecule across the other. In the present work, we extend this analysis to acene dimers up to $(\text{pentacene})_2$, to benzene on the surface of a $C_{96}H_{24}$ graphene nanoflake, and to corannulene dimer, which is less structurally rigid and bows significantly in its equilibrium geometry. In the course of this analysis, we also make the first detailed examination of the effects of charge penetration in these larger π-stacked systems.

We revisit the question of whether π-stacking constitutes an exceptional form of dispersion, using quantum-mechanical energy decomposition analysis based on symmetry-adapted perturbation theory (SAPT).[21,49–52] Side-by-side comparison of results for PAHs with their saturated polycyclic analogues (fused cyclohexane ring systems) reveals that there are indeed unique aspects of dispersion interactions in aromatic systems. These feature ultimately originate in the fact that PAHs are planar and structurally rigid, which facilitates exceptionally close-contact interactions *via* vdW forces. In this close-contact regime, electrostatic interactions become attractive even in cofacial geometries where they might be asymptotically repulsive. At the intermolecular separations that typify π-stacking, the interaction potential is dominated by vdW effects that drive charge penetration, nullifying the classical electrostatic picture. This implies that π-stacking is not solely attributable to a unique form of dispersion, but conspires with molecular geometry to afford a unique combination of electrostatic attraction and the vdW interactions in flat, rigid molecules.

2 Computational details

Interaction energies are calculated using the extended "XSAPT" version of second-order SAPT,[52–54] which includes a variational description of polarization for electrostatics.[55] Monomer wave functions were computed using the LRC-ωPBE functional,[56,57] tuning the range-separation parameter ω as described in previous work.[52,57] Tuned values of ω can be found in Table S1 (ESI†).

Induction energies reported here include a "δE_{HF}" correction,[50] in which a Hartree–Fock calculation for the dimer is used to estimate polarization beyond second order in perturbation theory. In results presented below, the induction (or polarization) energy is defined as

$$E_{ind} = E_{ind}^{(2)} + E_{exch\text{-}ind}^{(2)} + \delta E_{HF} \quad (2)$$

where $E_{ind}^{(2)}$ and $E_{exch\text{-}ind}^{(2)}$ are the second-order SAPT induction and exchange-induction components. First-order SAPT electrostatics ($E_{elst}^{(1)}$, eqn (1)) and exchange ($E_{exch}^{(1)}$) energies will simply be reported as E_{elst} and E_{exch}, respectively.

In place of the usual second-order SAPT dispersion terms, which tend to be the least accurate contributions to the second-order version of the theory,[53,57,58] we use a self-consistent many-body dispersion (MBD) method,[59] which is a modified form of the MBD approach introduced by Tkatchenko *et al.* for use with density functional theory.[60–62] The MBD formalism goes beyond an atomic-pairwise description of dispersion to include screening effects between multiple polarizable atomic centers in a self-consistent fashion, which is likely to be important for conjugated π-electron systems.[63] Combined with electrostatic, induction, and Pauli repulsion energies computed using SAPT, the resultant XSAPT+MBD method is a computationally efficient way to calculate benchmark-quality noncovalent interaction energies in large supramolecular complexes.[55,59] These calculations were performed using Q-Chem v. 5.3.[64]

Geometries for all complexes were optimized at the TPSS-D3/def2-TZVP level of theory,[65,66] and are unconstrained except where noted. (Constrained optimizations are reported for corannulene dimer and these were performed using the ORCA software, v. 4.1.1.[67]) In order to account for deformation in the large graphene flake that is considered here, geometries of the $(C_{96}H_{24})\cdots(C_6H_6)$ complex were optimized at each point on a two-dimensional potential energy surface, essentially scanning the center position of C_6H_6 over the two-dimensional plane of $C_{96}H_{24}$. Potential energy surfaces for the naphthalene and decalin (perhydronaphthalene) dimers, computed along a two-dimensional cofacial sliding coordinate, do not include monomer deformation. In these cases, a parallel configuration is used with a face-to-face separation of 3.4 Å for $(\text{naphthalene})_2$ and 4.6 Å for $(\text{decalin})_2$.

3 Results and discussion

A large body of research on π–π interactions has focused on benzene dimer, both because it is amenable to high-level *ab initio* calculations and because it is regarded as emblematic of π-stacking. Conformational preferences in $(C_6H_6)_2$ are framed as a competition between London dispersion, favoring the cofacial π-stacked arrangement (Fig. 1a), and quadrupolar electrostatics that favor a perpendicular configuration (Fig. 1c).[10,11,15] Accurate calculations suggest that these two configurations are nearly isoenergetic,[13,30–33] and indeed the short-range structure of liquid benzene that is inferred from neutron diffraction experiments is consistent with the coexistence of both orientations.[68]

It happens that the interaction energy (stacking energy) in benzene dimer is nearly identical to that of cyclohexane dimer.[69] This raises the question of whether the former is representative of π–π interactions more generally, or indeed

 This journal is © the Owner Societies 2020

Published on 13 October 2020. Downloaded on 11/11/2020 5:31:14 PM.

whether such interactions are genuinely distinct from "ordinary" (and ubiquitous) London dispersion.[1,7] In arguing that they are not, it is sometimes pointed out that C_6H_{12} has a larger (isotropic) polarizability as compared to C_6H_6,[7] although this argument misses the point that polarizability is an extensive quantity and the polarizability per electron is slightly larger in C_6H_6 than it is in C_6H_{12}.[70] This observation suggests that in comparing aromatic to saturated hydrocarbons, a comparison of size-dependent trends may afford insight, and this is what we consider first.

3.1 Size-dependent trends

We first examine size-dependent trends amongst dimers of linear acenes, $(C_{4n+2}H_{2n+4})_2$, with the number of rings ranging up to $n = 5$ (pentacene). Both perpendicular and parallel-offset geometries are considered, as shown in Fig. 2. We also consider dimers of the complementary polycyclic saturated hydrocarbon (PSH) molecules, the perhydroacenes, ranging from cyclohexane dimer through perhydropentacene dimer, $(C_{22}H_{36})_2$. Interaction energies of the linear acenes have been reported elsewhere,[1,71] and our XSAPT+MBD interaction energies are in line with previous computational work.

The present calculations capture the energetic similarities that are expected in the single-ring systems,[69] as the stacking energies of benzene and cyclohexane dimers are within 0.1 kcal mol^{-1} of one another. This degeneracy is lifted when just one more ring is added, as the parallel-offset geometry of naphthalene dimer emerges as the most stable of the two-ring structures depicted in Fig. 2, by 1.3 kcal mol^{-1}. This prediction is corroborated by experimental neutron diffraction data for liquid naphthalene, which exhibit a clear propensity for parallel-offset configurations,[72] unlike the corresponding data for liquid benzene.[68]

Evolution of the size dependence of the interaction energies is presented in Fig. 3a. These data demonstrate that enhanced attraction with respect to the length of the acene nanoribbon is unique to the cofacial arrangement of these aromatic dimers; interaction energies for perpendicular configurations of the PAH dimers remain nearly identical to those for the stacked PSH dimers even as the size of the monomer unit is increased. In contrast, intermolecular attractions in the parallel-offset PAHs is amplified with the addition of each ring until the energy difference between parallel-offset $(pentacene)_2$ and the other two $n = 5$ ring systems (perpendicular pentacene dimer and stacked perhydropentacene dimer) exceeds 6 kcal mol^{-1}.

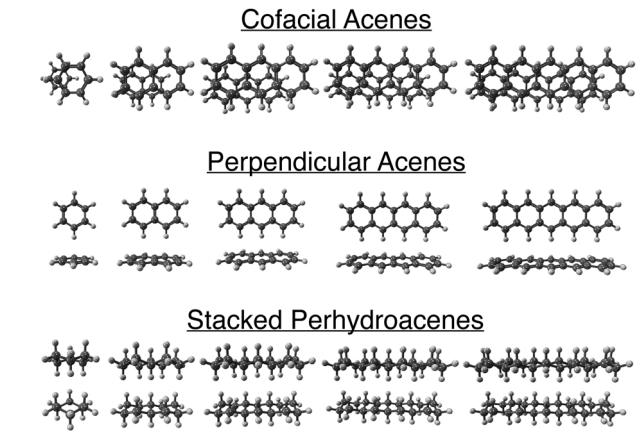

Fig. 2 Optimized geometries of acene dimers in parallel-offset (top) and perpendicular (middle) geometries, and stacked dimers of their saturated polycyclic hydrocarbon analogues (bottom).

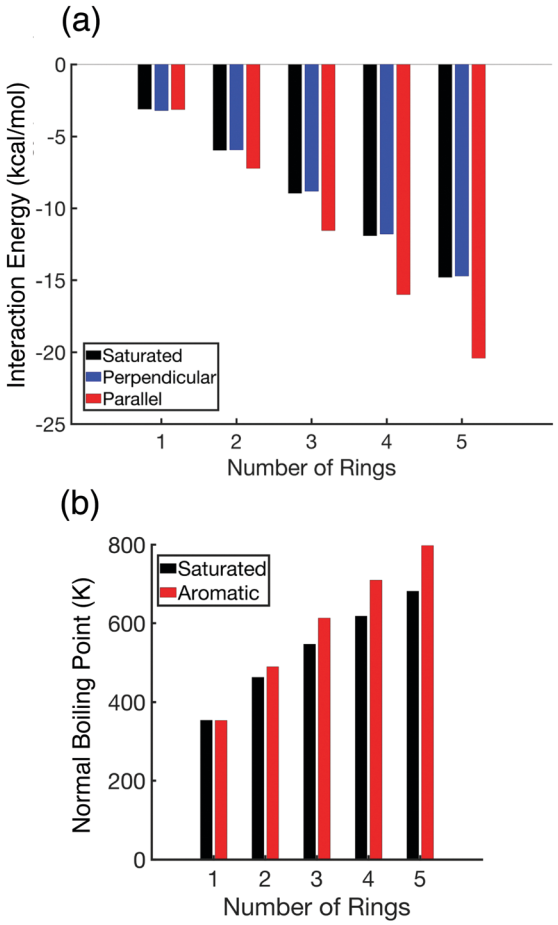

Fig. 3 (a) XSAPT+MBD interaction energies for the acenes (in both parallel and perpendicular orientations) and their saturated analogues, the perhydroacenes. (b) Experimental boiling points for acenes and their saturated analogues, from ref. 73.

All else being equal, stronger intermolecular attraction means larger enthalpy of vaporization and this is reflected in the boiling-point data presented in Fig. 3b. Remarkably, these experimental data capture the similarity between interaction energies for the benzene and cyclohexane dimers, as well as the fact that adding just one ring lifts the degeneracy; the boiling point of naphthalene exceeds that of perhydronaphthalene (decalin) by 27 K. The boiling points of the aromatics increase more rapidly *versus* monomer size as compared to those for the saturated hydrocarbons. In view of the neutron diffraction data for liquid benzene[68] and liquid naphthalene,[72] which provide evidence for both parallel and perpendicular orientations in the former case but only parallel configurations in the latter, it seems reasonable to hypothesize that the boiling point increases for

Published on 13 October 2020. Downloaded on 11/11/2020 5:31:14 PM.

larger PAHs evidence a continued propensity for parallel-offset geometries in aromatics larger than benzene.

Together, these data suggest that $(C_6H_6)_2$, rather than being a paradigmatic example, is actually a poor surrogate for aromatic π–π interactions more generally. This is consistent with studies of the size-dependent trends in $(benzene)_2$, $(naphthalene)_2$, and $(pyrene)_2$ interaction energies,[42] where it was determined that extrapolations based on smaller PAHs produces misleading results. Grimme has also suggested that any "special" aspects of dispersion in π–π interactions manifest only in aromatic moieties larger than a single benzene ring.[1] The present results are consistent with that idea but suggest that the aromatic moiety need not be much larger. Cofacial π-stacking rapidly comes to dominate the intermolecular landscape of the acene dimers as the length of the nanoribbon increases, with a widening energetic gap between the parallel-offset and the perpendicular arrangement.

3.2 Benzene on graphene

We next investigate π-stacking in a system with disparate monomer sizes, examining the two-dimensional potential energy surface for scanning C_6H_6 over the surface of a graphene nanoflake ($C_{96}H_{24}$), in both cofacial and perpendicular orientations. There are no near-degeneracies in this case (see Fig. 4), and a comparison between the minimum-energy structure obtained in either orientation reveals that the cofacial arrangement is 6 kcal mol^{-1} more stable than the perpendicular configuration. The cofacial benzene probe is more stable when the center of the ring is directly atop an atom or bond of the underlying $C_{96}H_{24}$ molecule, because these configurations minimize the effects of exchange repulsion. This is the benzene-graphene analogue of the parallel-offset geometry in the acene dimers, and it arises for the same reasons that we have previously discussed for the benzene and anthracene dimers.[29] In the perpendicular orientation, benzene on $C_{96}H_{24}$ adopts a minimum-energy geometry in which the C–H bond of benzene points to the center of a ring on $C_{96}H_{24}$, analogous to the T-shaped isomer of $(C_6H_6)_2$.

In previous work,[29] we developed an analytic model potential for describing π–π interactions, to serve as a replacement for the conventional Hunter–Sanders model.[11] Whereas the latter consists of an attractive London dispersion term along with point charges arranged to provide repulsive quadrupolar electrostatics, we called our analytic model a "vdW potential" because it replaces the electrostatics with an overlap-based model of Pauli repulsion. (Short-range repulsion plus long-range dispersion are the intermolecular forces that compete to yield the vdW equation of state for gases, so the nomenclature is consistent.) For the dispersion component of this vdW model, we used a pairwise atomic dispersion potential fit to *ab initio* dispersion data.[52]

Potential surfaces for the $(C_6H_6)\cdots(C_{96}H_{24})$ system, generated by both of these model potentials, can be found in Fig. S1 and S2 (ESI†). The Hunter–Sanders model erroneously predicts an energy minimum in which benzene sits directly above the center ring of $C_{96}H_{24}$ (*i.e.*, cofacial rather than offset stacking), at odds with the XSAPT+MBD results. In contrast, the vdW model correctly predicts that this configuration is a saddle point. The remainder of the two-dimensional XSAPT+MBD potential surface is also reproduced with high fidelity by the vdW model. Although in its present form this model is a simple parameterization designed for physical insight, it has a functional form amenable to use with classical force fields, to obtain interaction potentials for π-stacking with correct underlying physics.

Note that the minimum-energy point on both the parallel and perpendicular $(C_6H_6)\cdots(C_{96}H_{24})$ potential energy surfaces places the benzene molecule near the center of the graphene flake. In this sense, there is no analogue of the parallel-offset structure in $(C_6H_6)_2$, where one aromatic molecule extends beyond the edge of the other, although the driving force for off-center stacking in benzene-graphene is the same as that which drives the benzene dimer into a parallel-displaced geometry. Relative to the perpendicular arrangement, the cofacial orientation is strongly preferred in benzene-graphene, just as it was in acene dimers larger than $(C_6H_6)_2$.

A similar preference for π-stacked geometries has been noted in the case of $(C_6H_6)\cdots(C_{60})$,[74] implying that benzene's interactions with larger aromatic molecules more generally favor a π-stacked arrangement. Whereas the T-shaped and

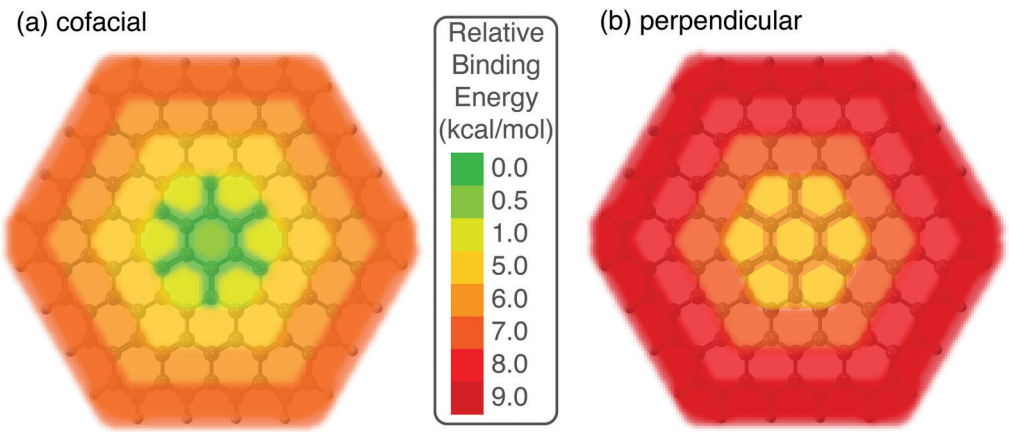

Fig. 4 Two-dimensional interaction potentials for a benzene molecule scanned along the surface of $C_{96}H_{24}$, which is shown, in either (a) a cofacial orientation or (b) a perpendicular orientation. Energies are reported relative to the most stable point on the cofacial potential surface.

 This journal is © the Owner Societies 2020

Published on 13 October 2020. Downloaded on 11/11/2020 5:31:14 PM.

parallel-offset geometries of $(C_6H_6)_2$ have nearly identical interaction energies, this degeneracy is a finite-size effect because the slip-stacked arrangement must sacrifice attractive dispersion, which falls off rapidly as the π-electron clouds of the two monomers are displaced from one another. On the surface of the graphene nanoflake, however, a small offset can be introduced without loss of dispersion, and the cofacial orientation becomes strongly preferred with respect to the perpendicular arrangement. Charge penetration effects, and therefore electrostatic interactions, are also essentially unchanged by this small displacement, which serves to reduce Pauli repulsion and thus to enhance the total interaction energy. The interaction potential of perpendicular benzene on $C_{96}H_{24}$ is not enhanced by parallel offsets. Maximizing the surface area of closely-interacting π-electron densities, "serving up the interactions on a platter", seems to be highly beneficial when extended π networks are considered, a fact that could not have been inferred from $(C_6H_6)_2$.

3.3 Size-intensive energy decomposition

Dispersion is intimately tied to polarizability but this connection has sometimes been misconstrued in the context of π–π interactions, with the somewhat larger polarizability of C_6H_{12} as compared to C_6H_6 taken as evidence that dispersion interactions in benzene dimer should not be larger than those in cyclohexane dimer.[7] Setting aside the fact that the polarizability per electron is actually larger in C_6H_6,[70] even this simple argument fails to generalize to monomers with more than one ring: the isotropic polarizability $\bar{\alpha}$ of naphthalene is (slightly) larger than that of perhydronaphthalene.[70] Furthermore, XSAPT+MBD calculations afford a dispersion energy of $E_{disp} = -5.8$ kcal mol^{-1} for $(C_6H_{12})_2$, which is less attractive than the value $E_{disp} = -6.7$ kcal mol^{-1} that is obtained for $(C_6H_6)_2$.

Clearly, polarizability is not the whole story when it comes to dispersion. Normalizing to the number of electrons (n_{elec}), so as to obtain a size-intensive property $\bar{\alpha}/n_{elec}$, isotropic polarizabilities per electron in benzene and cyclohexane are within 5% of one another, yet the dispersion energy in $(C_6H_6)_2$ is 16% larger than that in $(C_6H_{12})_2$. This means that the dispersion per electron,

$$\tilde{E}_{disp} = E_{disp}/n_{elec}, \quad (3)$$

is 33% larger in $(C_6H_6)_2$ that it is in $(C_6H_{12})_2$! The size-extensive nature of dispersion is familiar to any chemist in the guise of melting and boiling points for the *n*-alkanes that increase as a function of molecular weight, and this extensivity means that it is imperative to analyze dispersion on a per-electron basis when assessing trends *versus* molecular size. Only then can one make a valid comparison that might reveal whether π–π interactions constitute a unique form of dispersion.

Before doing so, let us define several relevant energy components. As in previous work,[29] we group together the SAPT electrostatic and induction energies, $E_{elst+ind} = E_{elst} + E_{ind}$. This "elst + ind" energy represents the sum of permanent and induced electrostatics. We also define the vdW energy to be the sum of the SAPT exchange and MBD dispersion energies,

$$E_{vdW} = E_{exch} + E_{disp}. \quad (4)$$

This is the part of the interaction potential that drives offset π-stacking.[29] The total interaction energy is

$$E_{int} = E_{elst+ind} + E_{vdW}. \quad (5)$$

To make a valid side-by-side comparison of energy components in homologous systems of increasing size, however, we must normalize by the number of particles. As we did for dispersion in eqn (3), we therefore we define a normalized (per-electron) vdW energy,

$$\tilde{E}_{vdW} = E_{vdW}/n_{elec}, \quad (6)$$

and also a normalized elst + ind energy,

$$\tilde{E}_{elst+ind} = E_{elst+ind}/(n_{nucl} + n_{elec}). \quad (7)$$

In eqn (7), we normalize by the total number of charged particles, because $E_{elst+ind}$ contains contributions from both nuclei and electrons. These normalized energy components are plotted in Fig. 5 for both acene and perhydroacene dimers.

As the size of the system increases, $\tilde{E}_{vdW}$ converges rapidly to a constant in all three cases considered: cofacial PAHs, perpendicular PAHs, and stacked PSHs. For acenes larger than naphthalene, it is perhaps surprising to observe that the value of $\tilde{E}_{vdW}$ is the same in both parallel and perpendicular orientations, even though the dispersion per electron ($\tilde{E}_{disp}$, Fig. 5b) is significantly larger in the parallel orientation. This is a result of significant cancellation between the dispersion and exchange-repulsion energies, as has been noted in other work on π-stacking, where this observation is sometimes used to conclude that the geometry must be controlled by electrostatics.[16,75] However, our work suggests that it is often E_{vdW}, not E_{elst} or $E_{elst+ind}$, that dictates the geometry.[29] Because the attractive dispersion and repulsive exchange energies are the largest energy components for close-contact π–π interactions, and because the forces on the nuclei must be zero at the equilibrium geometry, it is essentially a requirement that dispersion and exchange repulsion cancel to a significant extent at the equilibrium geometry, meaning that their sum (E_{vdW}) is small. As such, the fact that E_{vdW} is small for equilibrium geometries should not be misconstrued to mean that vdW forces do not play an important role in dictating geometries. That assessment can properly be made only by examining potential energy surfaces, not simply by performing energy decomposition analysis at stationary points.

Whereas the per-electron vdW interactions effectively contribute a constant to the normalized (per-particle) interaction energy, the elst + ind energy makes a significant contribution in cofacial acenes that is absent in the perpendicular orientation, and also absent in the stacked perhydroacenes (Fig. 5a). In the latter two cases, $\tilde{E}_{elst+ind}$ converges rapidly to a limiting value as a function of molecular size, and in fact for the perpendicular acene dimers the value of $\tilde{E}_{elst+ind}$ has reached its converged value already in the case of benzene dimer. For the cofacial acene dimers, however, $\tilde{E}_{elst+ind}$ continues to grow as a function of molecular size and may not yet have reached its converged value even for $(pentacene)_2$.

Note that $E_{elst+ind}$ is attractive for the cofacial PAHs even though the classical quadrupole–quadrupole energy would be

Published on 13 October 2020. Downloaded on 11/11/2020 5:31:14 PM.

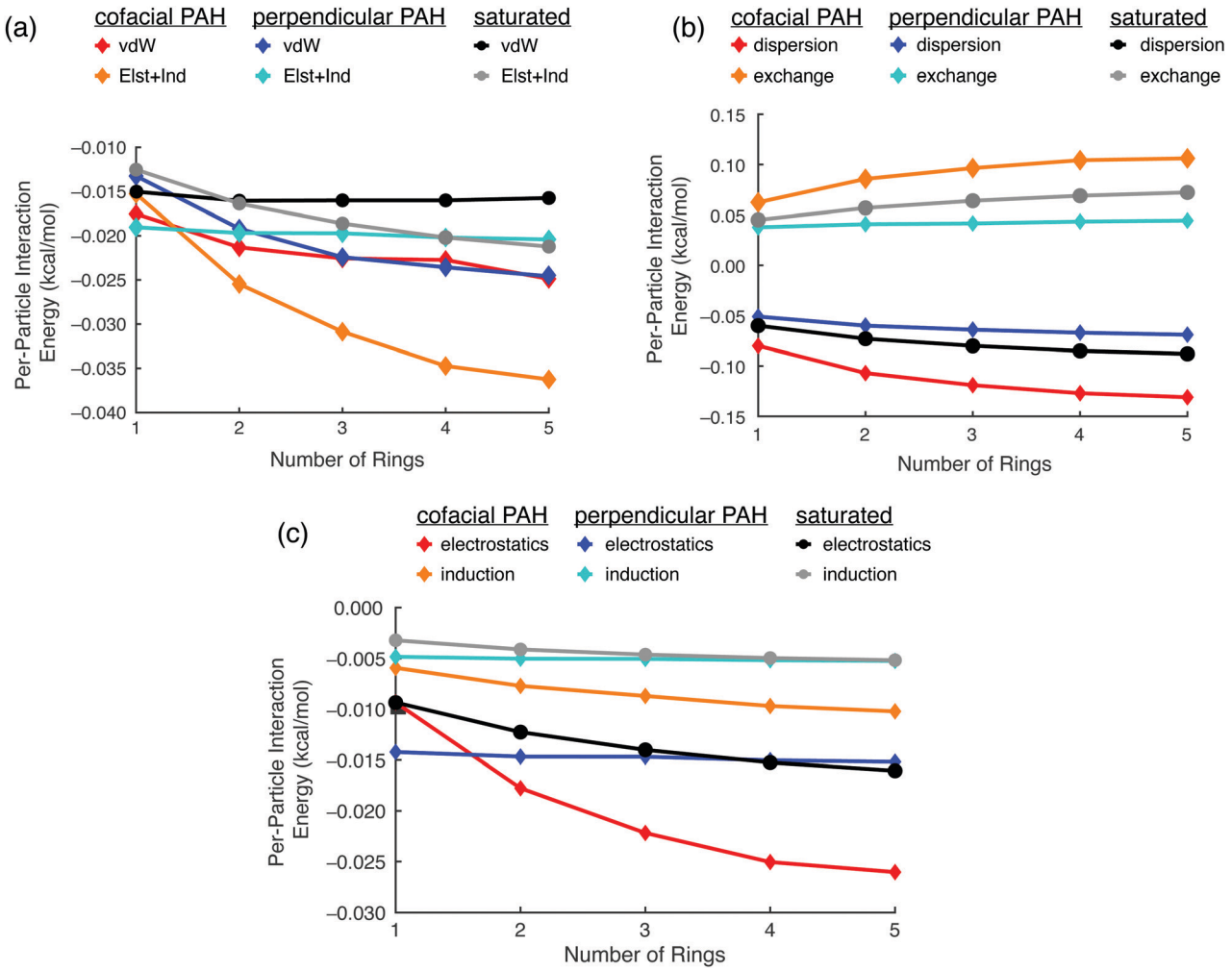

Fig. 5 Normalized interaction energy components in acene and perhydroacene dimers. (a) Plots of $\tilde{E}_{vdW} = E_{vdW}/n_{elec}$ and $\tilde{E}_{elst+ind} = E_{elst+ind}/(n_{nucl} + n_{elec})$, *versus* the size of the system measured by the number of rings. (b) Plots of $\tilde{E}_{vdW}$ separated into contributions from dispersion ($\tilde{E}_{disp} = E_{disp}/n_{elec}$) and from exchange ($\tilde{E}_{exch} = E_{exch}/n_{elec}$). (c) Plots of $\tilde{E}_{elst+ind}$ separated into contributions from permanent electrostatics [$\tilde{E}_{elst} = E_{elst}/(n_{nucl} + n_{elec})$] and from induction [$\tilde{E}_{ind} = E_{ind}/(n_{nucl} + n_{elec})$].

repulsive in this configuration. Apparently, this leading-order multipolar contribution is offset by charge-penetration effects arising from the close proximity of the two monomers at the vdW contact distance of the supramolecular complex. The quadrupolar electrostatic picture, and with it the Hunter–Sanders model, is therefore qualitatively wrong for these systems, as we documented previously for benzene dimer.[29]

Charge penetration decays exponentially with distance, in proportion to density overlap, which is smallest in the stacked PSHs due to their larger intermolecular separation ($\approx$4.6 Å, independent of monomer size). The average intermolecular separation in the cofacial acenes is $\approx$3.4 Å, making charge penetration much more significant. This is underscored by the normalized elst + ind energy, $\tilde{E}_{elst+ind}$, which changes by 67% between the cofacial benzene and naphthalene dimers. The corresponding change in the saturated systems is only 31% between cyclohexane and perhydronaphthalene.

A significant orientational effect is observed as well in the case of the acene dimers. The perpendicular configuration exhibits far less density overlap, and this manifests as a mere 3% change in $\tilde{E}_{elst+ind}$ between T-shaped $(benzene)_2$ and perpendicular $(naphthalene)_2$. Smaller charge-penetration effects in the perpendicular orientation explain why $\tilde{E}_{elst+ind}$ is essentially the same regardless of the length of the acene nanoribbon. This strong orientational dependence is imposed by the exponential dependence of charge penetration on density overlap, and dramatically alters the elst + ind interaction as the system moves from perpendicular to cofacial geometries. Dispersion may be the dominant intermolecular force in π-stacking, and its competition with exchange repulsion explains the emergence of offset-stacking, but the contributions of electrostatics and induction to the stability of π–π interactions cannot be ignored in larger aromatic systems. (We have argued that electrostatics can be ignored in benzene dimer,[29] which is one reason why this system is not representative of π–π interactions more generally.) Augmentation of $\tilde{E}_{elst+ind}$ in cofacial PAH dimers is a unique stabilization effect brought about by the interpenetration of π-electron densities, consistent with the

 This journal is © the Owner Societies 2020

Published on 13 October 2020. Downloaded on 11/11/2020 5:31:14 PM.

notion that π-stacking constitutes a unique form of intermolecular interaction.

3.4 Role of HOMO/LUMO gaps

An alternative hypothesis to explain the increase in $\tilde{E}_{\text{elst+ind}}$, as a function of monomer size, for the cofacial acene dimers is that it results from a narrowing of the gap between highest occupied and lowest unoccupied molecular orbitals. HOMO/LUMO gap for both the acenes and their perhydro analogues are plotted as a function of size in Fig. S3 (ESI†). While the gap decreases monotonically with size in both cases, it does so much more rapidly for the aromatic molecules. The calculated HOMO/LUMO gaps extrapolate to 0.6 eV (acene) and 8.8 eV (perhydroacene) for infinitely-long nanoribbons. The former value is consistent with a measured band gap of 0.2 eV PAH nanoribbons as thin as 15 nm,[76] and while these computed values cannot be equated directly with the band gaps of graphene and graphane, these extrapolations are at least suggestive of the difference between these materials. Experimentally measured band gaps are zero for graphene and 4 eV for graphane.[77,78]

Induction can be understood as occupied → virtual excitations engendered by the perturbing influence of the electrostatic potential from a neighboring molecule, and such excitations become more accessible as the HOMO/LUMO gap decreases. Therefore one might ask whether the growth in $\tilde{E}_{\text{elst+ind}}$ as a function of size (Fig. 5a) results from a gap-induced increase in $\tilde{E}_{\text{ind}}$. We address this hypothesis by separating $\tilde{E}_{\text{elst+ind}} = \tilde{E}_{\text{elst}} + \tilde{E}_{\text{ind}}$ and examining these components separately, in Fig. 5c. For the cofacial acene dimers, the per-particle electrostatic energy $\tilde{E}_{\text{elst}}$ is significantly larger than the per-particle induction energy $\tilde{E}_{\text{ind}}$, and also grows faster as a function of molecular size. This suggests that charge penetration effects, integrated over an increasingly long molecule and rendering the electrostatic energy increasingly attractive, are more important than the gap-induced increase in the induction energy. Size-dependent changes in $\tilde{E}_{\text{elst+ind}}$ therefore have less to do with band gaps and more to do with interpenetration of π-electron clouds.

While dispersion is exceptionally strong in cofacial PAHs, its influence is exhausted in the determination of the geometry of the system. The two monomers approach closely enough to balance dispersion with Pauli repulsion, and not closer, and the elst + ind interactions exist under the constraints of a vdW-driven geometry. For complexes consisting of flat, rigid, two-dimensional molecules, these constraints can be satisfied while retaining large density overlap. This observation bolsters the case that it is charge penetration, not dispersion, that provides the exceptional attraction in π–π systems. This should not, however, be misconstrued to mean that dispersion is less important than electrostatics in π-stacking. Without exceptionally strong dispersion, the vdW force would reach equilibrium at larger intermolecular separation, reducing charge penetration and making electrostatic interactions less favorable, even tending towards repulsive in the cofacial arrangement when the intermolecular separation is large. Instead, the π-stacking phenomenon should be understood as a dramatic increase in the electrostatic interaction that is facilitated by the unique vdW force and is only possible in complexes composed of rigid, two-dimensional molecules. The importance of planar geometries in facilitating strong dispersion is discussed in more detail in the next section.

Like induction, dispersion also relies on occupied → virtual excitations, and we have noted above that the per-electron dispersion interactions increase nonlinearly with monomer size. Even though dispersion is largely cancelled by exchange repulsion, $\tilde{E}_{\text{disp}}$ is slightly more attractive than $\tilde{E}_{\text{exch}}$ is repulsive, for all three sets of systems considered; see Fig. 5b. The change in $\tilde{E}_{\text{disp}}$ with monomer size is most pronounced for the cofacial acene dimers and is not due to any reduction in the intermolecular separation, which is 3.4 Å in both the benzene and pentacene dimers. HOMO/LUMO gaps, on the other hand, are 11.3 eV for benzene and 5.4 eV for pentacene. We conclude that the change in $\tilde{E}_{\text{disp}}$ is attributable primarily to the significant reduction in the gap, rather than any change in the intermolecular separation.

These intermolecular separations are consistent with the interlayer separation of 3.35 Å in graphene,[79] suggesting that the intermolecular distance between PAHs converges rapidly with monomer size. Such strong similarity, between the intermolecular separation in a system as small as $(\text{benzene})_2$ with the interlay spacing in graphitic carbon, provides further evidence that the dominant effect of a parallel offset is to mitigate exchange repulsion. If electrostatics were the driving force for offset-stacking, then the intermolecular separation in $(C_6H_6)_2$ would likely be very different from that in graphene.

3.5 Role of collective density oscillations

Electron energy-loss spectroscopy and atomic force microscopy reveal that the π electrons in PAHs behave like plasmons.[80,81] In graphene, these surface plasmons obey the typical dispersion relation for an ideal two-dimensional electron gas.[82] The two-dimensional collective motion of the plasmons in graphene is captured in the quantum harmonic oscillator model that is used in the MBD approach,[62] where it manifests as in-plane displacements of the oscillators.[46,47] These plasmon modes are the lowest-energy dispersive modes in π-stacked systems, and can be related to the HOMO → LUMO transition of PAHs in the molecular orbital picture. The lowest π → π* transitions in PAHs are in-plane excitations that lead to the diffusion of charge across the plane of the molecule, and the delocalized nature of the π electrons leads to low-energy HOMO → LUMO transitions at energies that vary inversely with the size of the PAH. Conversely, in the stacked perhydroacene dimers, the nodal structure of the σ orbitals prevents such delocalization, and the corresponding σ → σ* transition is out-of-plane and much higher in energy. Due to its three-dimensional shape, electrodynamic screening in graphane differs from that in graphene, causing the dispersion of plasmon waves through quasi-two-dimensional materials to be slowed.[83]

Fig. 6a and b show the lowest-energy coupled oscillator eigenmodes in $(C_6H_6)_2$ and $(C_6H_{12})_2$, obtained from the MBD model. Comparison of these modes suggests that dispersion in benzene dimer is facilitated by in-plane oscillations of the electrons, whereas in cyclohexane dimer the fluctuations are

Published on 13 October 2020. Downloaded on 11/11/2020 5:31:14 PM.

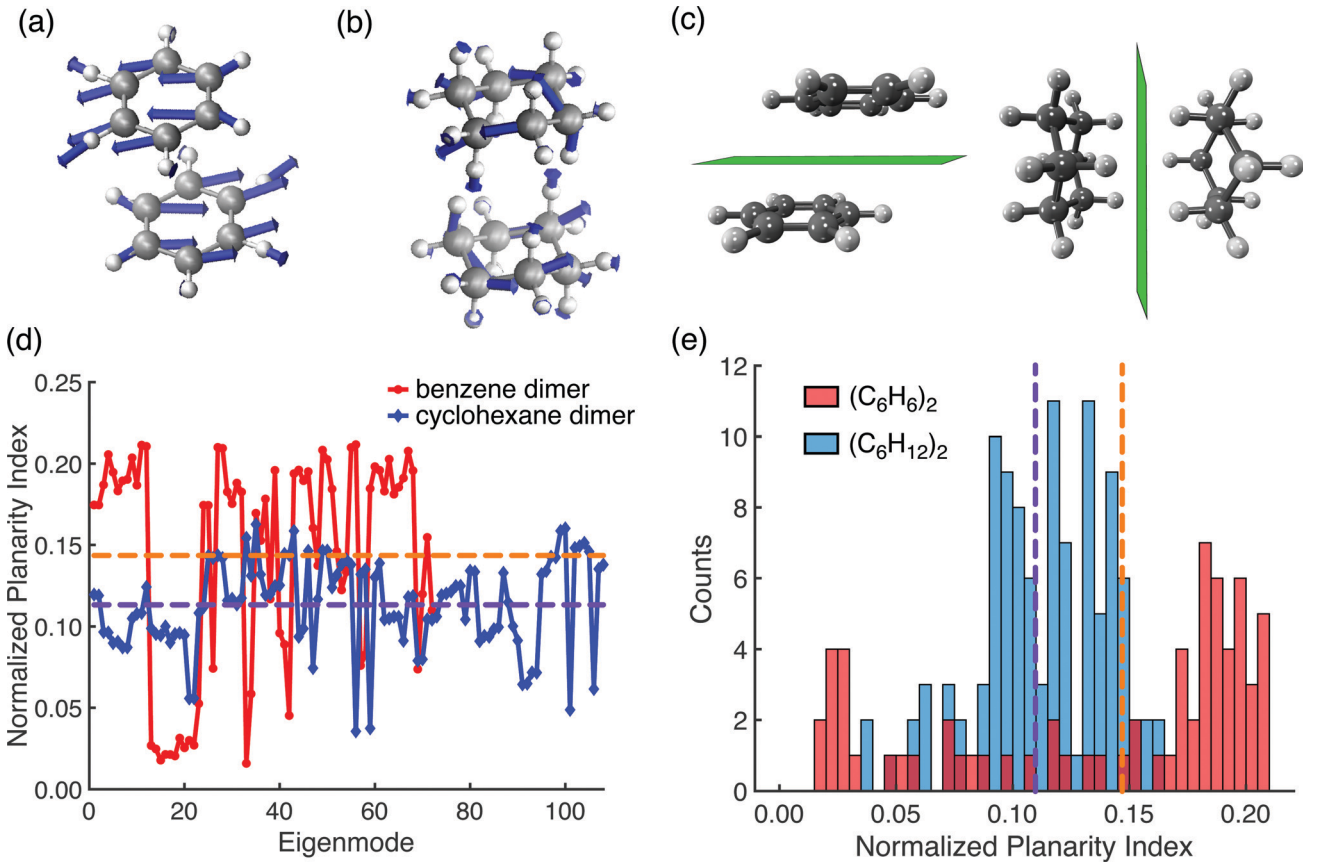

Fig. 6 Lowest-energy coupled quantum harmonic oscillator modes, corresponding to the eigenvectors of the coupled MBD Hamiltonian, for (a) π-stacked benzene dimer and (b) stacked cyclohexane dimer. The planarity of each eigenmode is measured using oscillator displacements relative to the planes in (c), resulting in a normalized planarity index (NPI) for each mode that is shown in (d). A histogram of the NPIs is depicted in (e). The orange and purple dashed lines in (d) and (e) indicate the mean NPI for $(C_6H_6)_2$ and $(C_6H_{12})_2$, respectively.

much more disordered. Disorder implies less in-plane charge mobility, consistent with dispersion interactions in $(C_6H_{12})_2$ that arise from coupled out-of-plane $\sigma \rightarrow \sigma^*$ excitations.

These are qualitative comparisons based on just the lowest-energy eigenmode of the MBD Hamiltonian for each system, whereas in total there are $3 \times N_{\text{atoms}}$ separate modes in the spectrum, each of which contributes to the dispersion energy. In order to generalize and quantify the analysis above, we introduce a normalized planarity index (NPI) to assess the maximum planarity of each eigenmode. The NPI quantifies how much the atomic oscillator displacements for a given eigenmode deviate from the intermolecular planes that are suggested in Fig. 6c, with limiting values NPI = 1 if all of the displacements are parallel to the prescribed plane and NPI = 0 if they are all perpendicular to it. (Mathematical details are provided in the ESI†).

The individual NPIs for each of the $3N_{\text{atoms}}$ eigenmodes of the MBD Hamiltonian are plotted in Fig. 6d, for both $(C_6H_6)_2$ and $(C_6H_{12})_2$, and these values demonstrate that on average the excitations in $(C_6H_6)_2$ are 27% more planar than those in $(C_6H_{12})_2$, supporting the notion of greater in-plane charge displacement for dispersion interactions in benzene dimer. The distribution of NPIs for both systems is plotted in histogram form in Fig. 6e, from which we observe that the distribution of values is unimodal and centered around the mean in the case of $(C_6H_{12})_2$ but bimodal for $(C_6H_6)_2$. In the latter case, the distribution favors in-plane fluctuations, characterized by larger values of the NPI, although with a moderate preference for values NPI ≈ 0 and fewer data points at intermediate values. This hints that the dispersion-induced charge mobility in acenes is largely comprised of strongly in-plane and out-of-plane shifts, with little intermediate motion unlike the charge fluctuations that characterize $(C_6H_{12})_2$. The absence of these intermediate values of the NPI in the case of $(C_6H_6)_2$ is indicative of collective oscillation of charge, as modes that lie at the either end of the NPI distribution require oscillator displacements that are largely coplanar. In contrast, the charge displacements in cyclohexane dimer vary strongly from atom to atom.

This simple metric therefore allows for an assessment of collective charge fluctuations induced by dispersion, considering all eigenmodes on an equal footing. Dispersion-induced charge fluctuations in $(C_6H_6)_2$ have significantly more in-plane character as compared to those in $(C_6H_{12})_2$. The former are much more collective as well, implying that the charge distribution about each atom changes in the same way, in contrast to the disordered atomic-density perturbations in $(C_6H_{12})_2$.

 This journal is © the Owner Societies 2020

Published on 13 October 2020. Downloaded on 11/11/2020 5:31:14 PM.

Lastly, the per-electron dispersion energies for the PAHs ($\tilde{E}_{\mathrm{disp}}$, Fig. 5b) are also suggestive of collective excitations. A dispersion interaction requires creating an excitation, which creates a dipole moment even if no permanent dipole moment is present and gives rise to the induced-dipole picture of London dispersion. As such, larger values of $\tilde{E}_{\mathrm{disp}}$ reflect enhanced probability of collective excitation, even allowing for normalization for the size of the π system. The nonlinear increase in $\tilde{E}_{\mathrm{disp}}$ *versus* system size that is observed for the cofacial PAHs (Fig. 5b) can be understood to result from collective excitations that generate the aforementioned molecular plasmons. Even small graphene flakes (*i.e.*, acenes) thus appear to exhibit plasmon-like couplings in their dispersion interaction, whereas in the saturated hydrocarbons the planarity of the plasmon modes is disrupted. This result suggests that the dispersion in two-dimensional systems is unique, and changes as a function of the molecular geometry, adding additional evidence to support π-stacking as a unique form of noncovalent interaction.

3.6 Reduced density isosurfaces

In order to study the influence of dimensionality on intermolecular interactions, we next examine so-called "noncovalent interaction (NCI) plots",[84,85] *i.e.*, isosurfaces of the reduced density gradient

$$s(\mathbf{r}) = \frac{\|\hat{\nabla}\rho(\mathbf{r})\|}{2(3\pi^2)^{1/3}\rho(\mathbf{r})^{4/3}}. \quad (8)$$

The function $s(\mathbf{r})$ encodes information about intermolecular interactions because noncovalent interactions are characterized by regions where the density $\rho(\mathbf{r})$ is small (*i.e.*, away from the nuclei and the covalent bonds) yet rapidly varying, as a result of an antisymmetry requirement imposed by the existence of the molecule's noncovalent partner. Isosurfaces of $s(\mathbf{r})$ are plotted as in Fig. 7 for the cofacial and perpendicular acene dimers and for the stacked PSH dimers. For the cofacial acenes these isosurface plots reveal an incredibly flat landscape, and for the other two systems these isosurfaces bear a strong resemblance to plots of a vdW molecular surface. This is no accident, and results from the fact that the interactions are dominated by short-range exchange repulsion, without significant modulation by either electrostatics or induction.

Note that the density $\rho(\mathbf{r})$ that is used to obtain the plots in Fig. 7 does not include a self-consistent treatment of dispersion, so it is possible that these plots miss subtle changes in the density that are induced by dispersion. These self-consistent effects are found to be significant at metallic surfaces and interfaces,[86] but in the present cases the NCI plots are dominated by short-range vdW effects. For that reason, the NCI plots in Fig. 7 closely resemble molecular surface plots, *i.e.*, they resemble the contours of molecular shape. For these systems, the vdW interactions are maximally repulsive in the regions that correspond to the oscillations in the reduced density gradient.

For the cofacial PAHs, small ripples appear in the reduced density isosurface directly over the ring centers, indicating that the perfectly cofacial arrangement (with no offset) is less favorable as compared to a slip-stacked geometry. In contrast, a completely flat $s(\mathbf{r})$ isosurface would imply that the noncovalent interactions were such that the monomers have complete flexibility in their relative orientation, and indeed the isosurfaces for the cofacial PAHs are relatively flat as compared to those for either the perpendicular acene dimers or for the stacked PSH dimers. This reflects the fact that the cofacial acene dimers have the flexibility to adopt parallel-offset geometries that are sterically inaccessible to the PSH dimers, which are instead conformationally locked into place, as can be inferred from the highly corrugated $s(\mathbf{r})$ isosurfaces for the latter species. Parallel-offset geometries in cofacial PAHs minimize exchange repulsion, allowing for a slight decrease in intermolecular separation, *e.g.*, 3.8 Å for the cofacial benzene dimer saddle point (Fig. 1a) *versus* 3.4 Å for the parallel-offset minimum (Fig. 1b).[29,32] This maximizes stabilization from charge penetration and dispersion.[29]

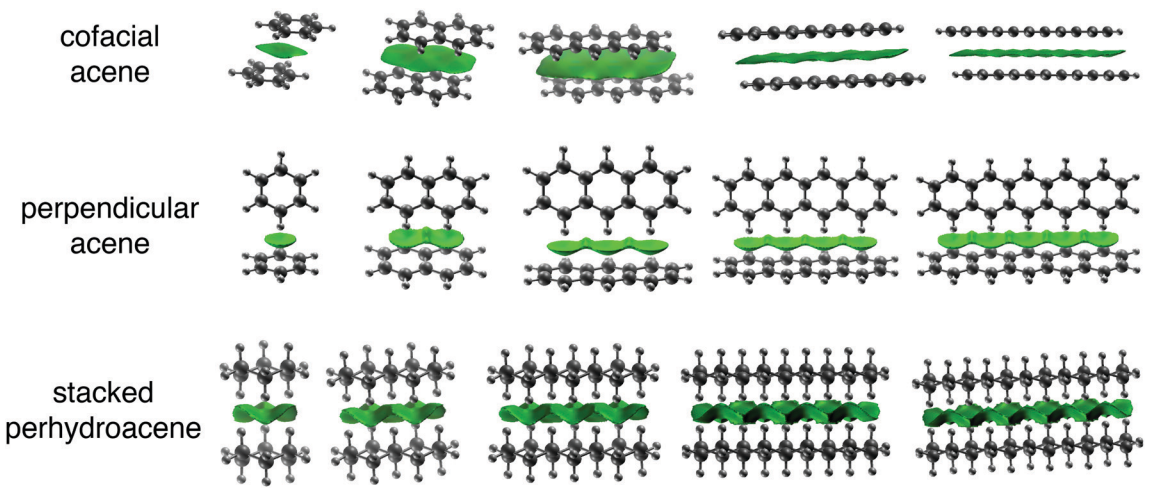

Fig. 7 Isosurfaces of the reduced density gradient $s(\mathbf{r})$ defined in eqn (8). These isosurfaces indicate regions of space where the electron density is small but rapidly varying, which is the signature of a noncovalent interaction.

Published on 13 October 2020. Downloaded on 11/11/2020 5:31:14 PM.

In contrast, stacked PSHs exhibit a single low-energy conformation characterized by interlocking C–H moieties on opposite monomers. This severely limits geometric flexibility along the parallel-sliding coordinate but also along the intermolecular coordinate, thus preventing the exploration of any closer-contact or slip-stacked geometries, which do not exist for these systems. Small corrugations can also be seen directly over C–C bonds in the perpendicular acene dimers, implying that exchange repulsion dominates the vdW interaction when the hydrogen atoms of one monomer are directly above the C–C bond density of the other monomer. These conclusions are consistent with the sawtooth potential energy surface of perpendicular anthracene dimer that we reported previously, using a vdW model potential.[29]

In the saturated hydrocarbons, the three-dimensional nature of the atomic framework results in geometric constraints that are more pronounced and that limit the capacity for intermolecular attraction, whereas the two-dimensional aromatic molecules can sidestep this steric hindrance by adopting a parallel-offset in the cofacial arrangement. In this sense, the geometry of the molecule (driven by aromaticity or lack thereof), along with the relative orientation of the π-electron densities, conspires with dispersion to afford a unique type of stacking interaction for the cofacial acene dimers that is not available to their perhydroacene analogues.

This line of argument suggests that it is the planarity of the PAHs, and not necessarily their aromaticity *per se*, that facilitates stacking interactions. This is consistent with other work suggesting that aromaticity is not a prerequisite for π-stacking, which can instead be driven other factors leading to a reduction in exchange repulsion.[2] Of course, aromatic molecules tend to be planar and rigid, which accounts for the close association between aromaticity and π-stacking. Planar molecules are better able to circumvent geometric constraints imposed by vdW interactions.

3.7 Energy landscapes for stacked polycyclic hydrocarbons

Isosurface plots of $s(\mathbf{r})$ in Fig. 7 afford a qualitative picture of the energy landscape along the cofacial sliding coordinate in these molecules. To obtain a more quantitative picture, we have computed the two-dimensional potential energy surface for cofacial sliding of $(\text{naphthalene})_2$ and $(\text{perhydronaphthalene})_2$; see Fig. 8. It proves illustrative to separate out the potential energy surface for Pauli repulsion, leaving

$$E_{\text{elst}} + E_{\text{ind}} + E_{\text{disp}} = E_{\text{int}} - E_{\text{exch}} \quad (9)$$

as the other potential energy surface in Fig. 8. Surfaces on the far left in Fig. 8 correspond to the left side of eqn (9).

Taken by itself, the $E_{\text{elst}} + E_{\text{ind}} + E_{\text{disp}}$ potential surface for $(\text{naphthalene})_2$ exhibits a preference for perfect cofacial stacking with no offset. (The $E_{\text{elst}} + E_{\text{ind}}$ potential surface, which is shown

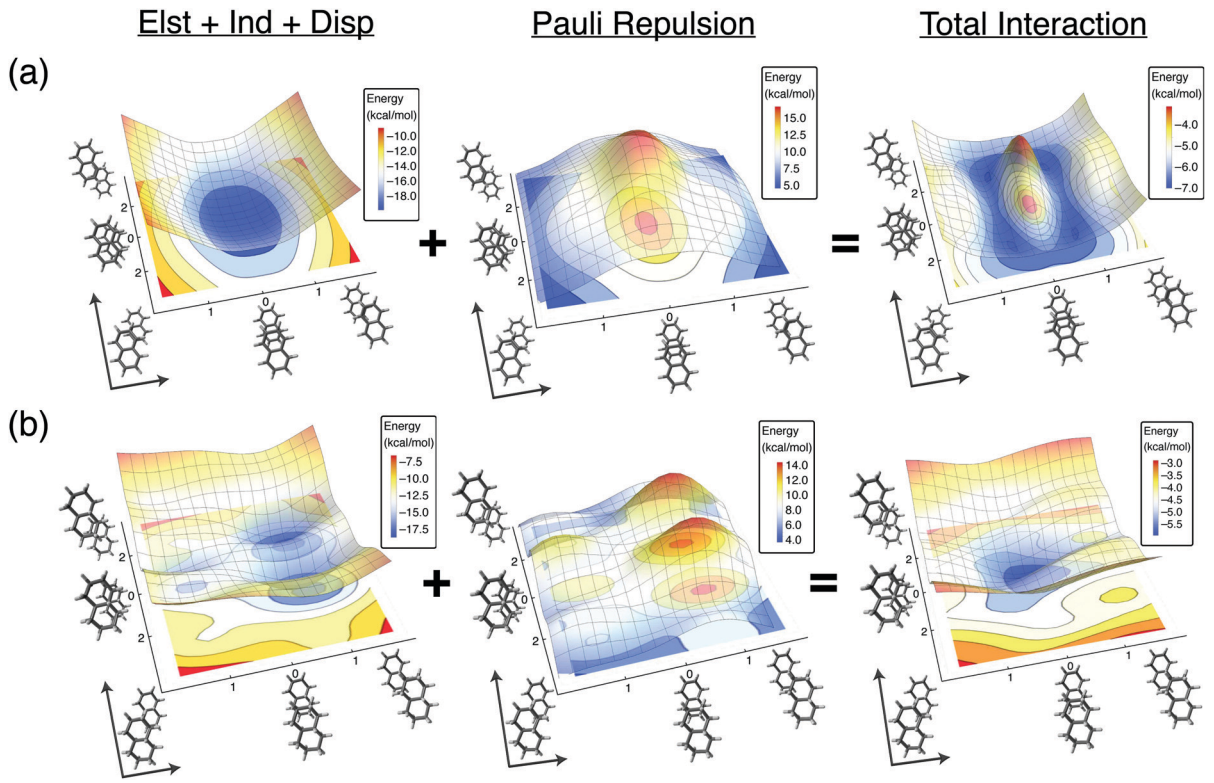

Fig. 8 Two-dimensional potential energy surfaces along the cofacial sliding coordinates of (a) $(\text{naphthalene})_2$ and (b) $(\text{perhydronaphthalene})_2$, at fixed intermolecular separation. Displacements along either axis are given in Ångstrom and illustrative geometric structures are shown. The surfaces on the left represent $E_{\text{int}} - E_{\text{exch}} = E_{\text{elst}} + E_{\text{ind}} + E_{\text{disp}}$. Adding the E_{exch} surfaces (middle) affords the total interaction energy surface (E_{int}, on the right). A two-dimensional contour plot is projected onto the plane of the coordinate axes in each case. Note that the energy scale varies in each plot, but in each case the most repulsive parts are shown in red and the most attractive regions are in blue.

 This journal is © the Owner Societies 2020

Published on 13 October 2020. Downloaded on 11/11/2020 5:31:14 PM.

in Fig. S4 (ESI†), has a saddle point at the cofacial geometry but this disappears when dispersion is added.) This is perfectly consistent with the vdW model of π–π interactions:[29] absent exchange repulsion, the interaction potential at fixed intermolecular separation is featureless and there is no driving force towards a parallel-offset geometry.

Interestingly, the $E_{elst} + E_{ind} + E_{disp}$ surface of (perhydronaphthalene)$_2$ exhibits three local minima corresponding to various parallel-offset structures. Each of these minima corresponds to a geometry that places hydrogen atoms from one monomer directly atop hydrogen atoms from the other. Geometries with overlapping out-of-plane atoms significantly amplify electrostatic charge penetration effects, but are also strongly prohibited by exchange repulsion. A similar phenomenon can be seen in the potential energy surface of perpendicular benzene dimer, where the L-shaped isomer (*i.e.*, the parallel-offset version of the T-shaped isomer) is a minimum on the $E_{elst} + E_{ind}$ potential surface.[29]

This nuanced structure is absent in the $E_{elst} + E_{ind} + E_{disp}$ surface of naphthalene dimer, as a result of enhanced dispersion and charge-penetration, both brought about by shorter intermolecular separation. In contrast to the Hunter–Sanders model, the sum of electrostatics (including induction) and dispersion predicts a qualitatively wrong minimum-energy geometry for this system! Exchange repulsion must be included to obtain the correct geometric structure, both for (naphthalene)$_2$, but also for its perhydro analogue. The exchange potentials in Fig. 8 highlight the importance of steric repulsion on the intermolecular geometry, as the most repulsive regions of E_{exch} are precisely the regions where $E_{elst} + E_{ind} + E_{disp}$ is most favorable. In (naphthalene)$_2$, Pauli repulsion shifts the geometry in a manner that corresponds to slip-stacking, whereas in (perhydronaphthalene)$_2$, E_{exch} shifts the geometry from a parallel-offset one to a structure with interlocking C–H moieties directed towards the centers of the rings on the other monomer. In this way, Pauli repulsion can be viewed as the sculptor of intermolecular orientation, especially in the short-range regime where classical electrostatic arguments are invalid.

A complementary point of view comes in noting that the $E_{elst} + E_{ind} + E_{disp}$ contribution to the interaction energy of naphthalene dimer is 14% less attractive at the actual minimum-energy (slip-stacked) geometry of the complex that it is at the perfectly cofacial geometry that the system would adopt in the absence of Pauli repulsion. For perhydronaphthalene dimer, the corresponding reduction is 21%. In other words, simply accounting for changes in geometry induced by exchange repulsion reduces the attractive components of the potential by these amounts, even before the repulsion energy itself is added into the mix. We find it notable that this geometric effect is less significant for the aromatic dimer. The relatively featureless nature of the $E_{elst} + E_{ind} + E_{disp}$ surface for naphthalene dimer means that the geometric displacement that is forced upon the system by the introduction of E_{exch} has a smaller impact on the attractive components of the interaction. The unsaturated system is more sensitive to the displacements produced by addition of Pauli repulsion.

Furthermore, the featureless nature of the $E_{elst} + E_{ind} + E_{disp}$ potential for (naphthalene)$_2$ enhances the attractive interactions due to the uniformity of the charge penetration across the potential surface. For the PSH systems, the monomers adopt three-dimensional shapes because the spatial variation of $\rho(\mathbf{r})$, and thus the electrostatic interactions, is more complicated, and the monomers use their flexibility to conform to the contours of the repulsive interactions. In this sense, molecules that "serve up their attractive interactions on a platter" (*i.e.*, a rigid two-dimensional shape driven by aromaticity, that can be rotated in space but not deformed) are more likely to engage in especially strong attractive interactions because the attractive components of the interaction potential are less perturbed by the influence of exchange on the geometry of the system.

3.8 Influence of monomer distortion: corannulene dimer

In an effort to more directly correlate the flat geometries of PAH monomers with their tendency to adopt parallel-offset π stacks, we have investigated the interaction energies of corannulene dimer, $(C_{20}H_{10})_2$, along a "flexing" coordinate corresponding to curvature of the monomers. Corannulene monomer is naturally bowl-shaped, and its dimer adopts a geometry consisting of concentric (or stacked) bowls with no offset. We optimized the geometry of the dimer under dihedral constraints, fixing the curvature of each monomer in the constrained system in increments, starting from the unconstrained bowl-shaped equilibrium structure and ending with completely planar monomers, corresponding to cofacial π-stacking. All of the optimized structures were initially in a cofacial, stacked arrangement, and to prevent optimization to saddle points we manually nudged one molecule in each structure to a small offset and re-optimized with constraints. All structures whose curvature was constrained at $<80\%$ of the equilibrium value optimized to parallel-offset geometries whose offset increased as the curvature was reduced toward planar monomers. The optimized structures are depicted at the top of Fig. 9 where the "flex coordinate" indicates the degree of curvature, with 0% corresponding to planar monomers and 100% corresponding to the fully-relaxed geometry of (corannulene)$_2$.

Fig. 9 also reports interaction energies along this flexing coordinate, which are then further decomposed into an elst + ind component (permanent electrostatics + induction) and a vdW component (dispersion + Pauli repulsion), according to eqn (5). These data reveal that the intermolecular attraction is actually most favorable ($E_{int} = -18.9$ kcal mol^{-1}) in the coplanar geometry, whereas the equilibrium bowl-shaped structure of the complex has a slightly less attractive interaction energy ($E_{int} = -17.7$ kcal mol^{-1}). The resolution to this apparent paradox is that the monomer deformation energy, which is not considered in the analysis shown in Fig. 9, is larger in the coplanar geometry.

Contrary to a previous assertion,[87] the large dipole moment of bowl-shaped corannulene (measured experimentally at 2.07 D[88]) does not appear to have a dominant effect on the behavior of the electrostatic interaction along the flexing coordinate. While this may seem surprising, it again speaks to the breakdown of the classical multipole picture at length scales representative of vdW close-contact distances. If the dipole moments of the corannulene monomers were the dominant effect, then the bowl-shaped

Published on 13 October 2020. Downloaded on 11/11/2020 5:31:14 PM.

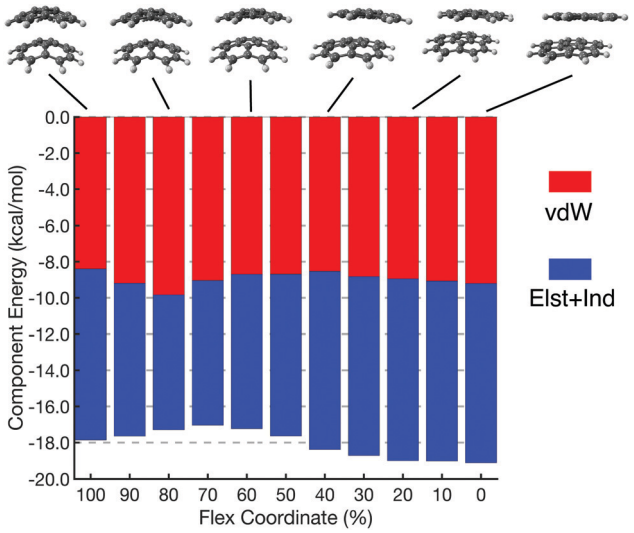

Fig. 9 Interaction energies for $(coranulene)_2$ along a "flexing" coordinate corresponding to curvature of the monomers. Illustrative geometries are shown, optimized at fixed curvature, with 100% flex corresponding to the fully-relaxed geometry of the dimer and 0% flex corresponding to enforced planarity of the monomers. The total length of each bar (red + blue) represents the total interaction energy, which is decomposed as $E_{int} = E_{vdW} + E_{elst+ind}$.

equilibrium structure would have the largest interaction energy or at least the largest elst + ind energy component. In fact, $E_{elst+ind}$ is more attractive (by 0.5 kcal mol^{-1}) in the coplanar, parallel-offset structure than it is in the fully-relaxed equilibrium geometry. The coplanar structure has quadrupole–quadrupole interactions but the monomer dipole moments are zero (by symmetry) in this configuration. As such, the enhanced elst + ind energy in the coplanar geometry signifies charge penetration effects leading to a breakdown of the classical dipolar picture along the flexing coordinate.

The dipole moment of corannulene in the equilibrium structure of the dimer is likely a consequence of the curvature of the monomers, rather than a driving force for adopting a curved geometry. There is a crossing point where sufficiently flat molecules will adopt a parallel offset, and at this point the balance of forces favors the formation of an offset. After this point there is also a monotonic increase in charge penetration as a function of flatness, as reflected by the additional electrostatic attraction. In this way, the formation of parallel offsets is a key feature of π-stacking, rather than some defect as the Hunter–Sanders picture would have it.

4 Conclusions

We have shown that π-stacking interactions in cofacial PAH dimers, the finite-size analogues of graphene layers, are stronger than the interactions in the corresponding polycyclic saturated hydrocarbons, which are analogues of graphane. The question is sometimes asked,[1,7] "does π-stacking constitute a unique form of dispersion?". Our answer is unequivocally "yes". That said, energetic stabilization due to dispersion is largely canceled by exchange repulsion in the determination of the geometry of the π-stacked complexes, which we believe should be a general feature of these systems. The exceptional strength of π-stacking interactions is better attributed to a special form of electrostatic attraction, caused by charge penetration and thus not captured by classical multipole moments, and which is furthermore unique to molecules with flat geometries. In PAHs, the planar geometry of the molecule acts in concert with the electrostatic interaction to enhance the attraction in a manner that is not available to polycyclic alkanes. The geometric flexibility of the latter causes them to hew closely to the contours of the vdW molecular surface that are established by the Pauli repulsion interaction, leading to a strong preference for structures with interlocking C–H moieties. The PAHs, in contrast, are characterized by π-electron densities that are effectively "served up on a pizza peel" that can be rotated but not distorted, and where closer intermolecular approach is possible, leading to significant enhancement of the electrostatic interaction. The lateral offsets ("slip-stacking"), by means of which the PAH dimers reduce Pauli repulsion, are unavailable to polycyclic molecules with three-dimensional geometries.

The role of charge penetration is especially important to acknowledge, and arguments based on classical multipoles badly misrepresent the interactions in π-electron systems. According to the widely-used Hunter–Sanders paradigm,[10,11,15] quadrupolar repulsion in cofacial π-stacked geometries competes with London dispersion, with the slip-stacked motif emerging as a compromise structure. At intermolecular distances characteristic of π-stacking interactions, however, the classical multipole description of electrostatics breaks down, and in fact there is no electrostatic driving force for offset-stacking.[29] This is true even in the corannulene dimer, which adopts the structure of concentric bowls whose curvature endows the monomers with sizable dipole moments of 2.07 D each. For benzene dimer, corannulene dimer, and numerous systems in between, we find that it is Pauli repulsion rather than electrostatics (or even electrostatics plus induction) that is responsible for offset-stacking. This explains, in particular, the frequent occurrence of offset-stacked geometries between nearby aromatic residues in protein structures,[8–10] across what must certainly be myriad electrostatic environments. Whatever may be happening with local electrostatics, Pauli repulsion is ever-present.

As we observed previously in smaller aromatic dimers,[29] the π-stacking interaction can be understood as a competition between dispersion (a fundamentally quantum-mechanical type of interaction, originating in electron correlation effects) and Pauli repulsion (also quantum-mechanical in origin, as a result of the exclusion principle). This, combined with the failure of any classical multipole description to rationalize either the geometric preferences of these systems or their strong electrostatic attraction, suggests that π-stacking is unique and intimately quantum-mechanical.

Moreover, the parallel-offsets adopted by supramolecular PAH architectures should not be viewed as defects or perturbations away from the π-stacked picture, but rather intrinsic to that picture. Interpenetration of the π-electron densities, driven by dispersion,

 This journal is © the Owner Societies 2020

Published on 13 October 2020. Downloaded on 11/11/2020 5:31:14 PM.

is key to making electrostatics attractive rather than repulsive in the cofacial orientations of these systems, but this comes at a price of increased Pauli repulsion. Offset-stacking mitigates that repulsion. This is facilitated by the planar geometries of PAHs, which also support collective excitations (plasmons) that are reflected in the nonlinear growth of the dispersion interaction in PAHs as a function of molecular size, even when normalized according to the number of electrons. Theory and experiment both suggest strong interactions in π systems that ought to be considered unique in their own right, as interactions that are "served up" on flat molecular architectures.

Conflicts of interest

J. M. H. serves on the board of directors of Q-Chem, Inc.

Acknowledgements

This work was supported by the U.S. Department of Energy, Office of Basic Energy Sciences, Division of Chemical Sciences, Geosciences, and Biosciences under Award No. DE-SC0008550. Calculations were performed at the Ohio Supercomputer Center under project no. PAA-0003.[89] K. C.-F. acknowledges a Presidential Fellowship from The Ohio State University.

Notes and references

1 S. Grimme, Do special noncovalent π–π stacking interactions really exist?, *Angew. Chem., Int. Ed.*, 2008, **47**, 3430–3434.
2 J. W. G. Bloom and S. E. Wheeler, Taking the aromaticity out of aromatic interactions, *Angew. Chem., Int. Ed.*, 2011, **50**, 7847–7849.
3 S. E. Wheeler, Understanding substituent effects in noncovalent interactions involving aromatic rings, *Acc. Chem. Res.*, 2013, **46**, 1029–1038.
4 T. Janowski and P. Pulay, A benchmark comparison of σ/σ and π/π dispersion: The dimers of naphthalene and decalin, and coronene and perhydrocoronene, *J. Am. Chem. Soc.*, 2012, **134**, 17520–17525.
5 M. R. Battaglia, A. D. Buckingham and J. H. Williams, The electric quadrupole moments of benzene and hexafluorobenzene, *Chem. Phys. Lett.*, 1981, **78**, 421–423.
6 J. H. Williams, The molecular electric quadrupole moment and solid-state architecture, *Acc. Chem. Res.*, 1993, **26**, 593–598.
7 C. R. Martinez and B. L. Iverson, Rethinking the term "pi-stacking", *Chem. Sci.*, 2012, **3**, 2191–2201.
8 G. B. McGaughey, M. Gagné and A. K. Rappé, π-Stacking interactions: Alive and well in proteins, *J. Biol. Chem.*, 1998, **273**, 15458–15463.
9 C. A. Hunter, J. Singh and J. M. Thornton, π–π interactions: The geometry and energetics of phenylalanine-phenylalanine interactions in proteins, *J. Mol. Biol.*, 1991, **218**, 837–846.
10 C. A. Hunter, K. R. Lawson, J. Perkins and C. J. Urch, Aromatic interactions, *J. Chem. Soc., Perkin Trans. 2*, 2001, 651–669.
11 C. A. Hunter and J. K. M. Sanders, The nature of π–π interactions, *J. Am. Chem. Soc.*, 1990, **112**, 5525–5534.
12 F. Cozzi, F. Ponzini, R. Annunziata, M. Cinquini and J. S. Siegel, Polar interactions between stacked π systems in fluorinated 1,8-diarylnaphthalenes: Importance of quadrupole moments in molecular recognition, *Angew. Chem., Int. Ed. Engl.*, 1995, **34**, 1019–1020.
13 E. C. Lee, D. Kim, P. Jurečka, P. Tarakeshwar, P. Hobza and K. S. Kim, Understanding of assembly phenomena by aromatic-aromatiic interactions: Benzene dimer and the substituted systems, *J. Phys. Chem. A*, 2007, **111**, 3446–3457.
14 I. Fleming, *Molecular Orbitals and Organic Chemical Reactions*, John Wiley and Sons, Chichester, United Kingdom, 2010.
15 D. E. Fagnani, A. Sotuyo and R. K. Castellano, π–π *Interactions, in Comprehensive Supramolecular Chemistry II*, Elsevier, Oxford, 2017, vol. 1, pp. 121–148.
16 E. M. Cabaleiro-Lago and J. Rodríguez-Otero, σ–σ, and π–π stacking interactions between six-membered cyclic systems. Dispersion dominates and electrostatics commands, *ChemistrySelect*, 2017, **2**, 5157–5166.
17 L.-J. Riwar, N. Trapp, B. Kuhn and F. Diederich, Substituent effects in parallel-displaced π–π stacking interactions: Distance matters, *Angew. Chem., Int. Ed.*, 2017, **56**, 11252–11257.
18 D. P. Malenov, A. J. Aladić and S. D. Zarić, Stacking interactions of borazine: Important stacking at large horizontal displacements and dihydrogen bonding governed by electrostatic potentials of borazine, *Phys. Chem. Chem. Phys.*, 2019, **21**, 24554–24564.
19 A. D. Glova, S. V. Larin, V. M. Nazarychev, J. M. Kenny, A. V. Lyulin and S. V. Lyulin, Toward predictive molecular dynamics simulations of asphaltenes in toluene and heptane, *ACS Omega*, 2019, **4**, 20005–20014.
20 M. Mousavi and E. H. Fini, Non-covalent π-stacking interactions between asphaltene and porphyrin in bitumen, *J. Chem. Inf. Model.*, 2020, DOI: 10.1021/acs.jcim.0c00507.
21 K. Patkowski, Recent developments in symmetry-adapted perturbation theory, *Wiley Interdiscip. Rev.: Comput. Mol. Sci.*, 2020, **10**, e1452.
22 M. O. Sinnokrot and C. D. Sherrill, Substituent effects in π–π interactions: Sandwich and T-shaped configurations, *J. Am. Chem. Soc.*, 2004, **126**, 7690–7697.
23 E. G. Hohenstein and D. C. Sherrill, Effects of heteroatoms on aromatic π–π interactions: Benzene-pyridine and pyridine dimer, *J. Phys. Chem. A*, 2009, **113**, 878–886.
24 E. G. Hohenstein, J. Duan and D. C. Sherrill, Origin of the surprising enhancement of electrostatic energies by electron-donating substituents in substituted sandwich benzene dimers, *J. Am. Chem. Soc.*, 2011, **133**, 13244–13247.
25 C. D. Sherrill, Energy component analysis of π interactions, *Acc. Chem. Res.*, 2013, **46**, 1020–1028.
26 R. M. Parrish and C. D. Sherrill, Quantum-mechanical evaluation of the π–π versus substituent–π interactions in π stacking: Direct evidence for the Wheeler-Houk picture, *J. Am. Chem. Soc.*, 2014, **136**, 17386–17389.
27 S. M. Ryno, C. Risko and J.-L. Brédas, Noncovalent interactions and impact of charge penetration effects in linear

Published on 13 October 2020. Downloaded on 11/11/2020 5:31:14 PM.

oligoacene dimers and single crystals, *Chem. Mater.*, 2016, **28**, 3990–4000.
28 G. Gryn'ova and C. Corminboeuf, Steric ''attraction'': Not by dispersion alone, *Beilstein, J. Org. Chem.*, 2018, **14**, 1482–1490.
29 K. Carter-Fenk and J. M. Herbert, Electrostatics does not dictate the slip-stacked arrangement of aromatic π–π interactions, *Chem. Sci.*, 2020, **11**, 6758–6765.
30 M. O. Sinnokrot and C. D. Sherrill, Highly accurate coupled cluster potential energy curves for the benzene dimer: Sandwich, T-shaped, and parallel-displaced configurations, *J. Phys. Chem. A*, 2004, **108**, 10200–10207.
31 M. O. Sinnokrot, E. F. Valeev and C. D. Sherrill, Estimates of the ab initio limit for π–π interactions: The benzene dimer, *J. Am. Chem. Soc.*, 2002, **124**, 10887–10893.
32 R. Podeszwa, R. Bukowski and K. Szalewicz, Potential energy surface for the benzene dimer and perturbational analysis of π–π interactions, *J. Phys. Chem. A*, 2006, **110**, 10345–10354.
33 O. Bludský, M. Rubeš, P. Soldán and P. Nachtigall, Investigation of the benzene-dimer potential energy surface: DFT CCSD(T) correction scheme, *J. Chem. Phys.*, 2008, **128**, 114102.
34 B. W. Gung and J. C. Amicangelo, Substituent effects in C_6F_6-C_6H_5X stacking interactions, *J. Org. Chem.*, 2006, **71**, 9261–9270.
35 S. Tsuzuki, T. Uchimaru and M. Mikami, Intermolecular interaction between hexafluorobenzene and benzene: Ab initio calculations including CCSD(T) level electron correlation correction, *J. Phys. Chem. A*, 2006, **110**, 2027–2033.
36 W. Wang, Y. Zhang and Y.-B. Wang, Highly accurate benchmark calculations of the interaction energies in the complexes $C_6H_6\cdots C_6X_6$ (X = F, Cl, Br, and I), *Int. J. Quantum Chem.*, 2017, **117**, e25345.
37 S. E. Wheeler and K. N. Houk, Origin of substituent effects in edge-to-face aryl–aryl interactions, *Mol. Phys.*, 2009, **107**, 749–760.
38 S. E. Wheeler and K. N. Houk, Substituent effects in the benzene dimer are due to direct interactions of the substituents with the unsubstituted benzene, *J. Am. Chem. Soc.*, 2008, **130**, 10854–10855.
39 S. E. Wheeler and K. N. Houk, Through-space effects of substituents dominate molecular electrostatic potentials of substituted arenes, *J. Chem. Theory Comput.*, 2009, **5**, 2301–2312.
40 S. E. Wheeler, Local nature of substituent effects in stacking interactions, *J. Am. Chem. Soc.*, 2011, **133**, 10262–10274.
41 S. E. Wheeler and J. W. G. Bloom, Toward a more complete understanding of noncovalent interactions involving aromatic rings, *J. Phys. Chem. A*, 2014, **118**, 6133–6147.
42 R. Podeszwa and K. Szalewicz, Physical origins of interactions in dimers of polycyclic aromatic hydrocarbons, *Phys. Chem. Chem. Phys.*, 2008, **10**, 2735–2746.
43 K. U. Lao and J. M. Herbert, Energy decomposition analysis with a stable charge-transfer term for interpreting intermolecular interactions, *J. Chem. Theory Comput.*, 2016, **12**, 2569–2582.
44 R. J. Wheatley and S. L. Price, An overlap model for estimating the anisotropy of repulsion, *Mol. Phys.*, 1990, **69**, 507–533.
45 J. H. Jensen and M. S. Gordon, An approximate formula for the intermolecular Pauli repulsion between closed shell molecules, *Mol. Phys.*, 1996, **89**, 1313–1325.
46 A. Ambrosetti, N. Ferri, R. A. DiStasio Jr. and A. Tkatchenko, Wavelike charge density fluctuations and van der Waals interactions at the nanoscale, *Science*, 2016, **351**, 1171–1176.
47 J. Hermann, D. Alfè and A. Tkatchenko, Nanoscale π–π stacked molecules are bound by collective charge fluctuations, *Nat. Commun.*, 2017, **8**, 14052.
48 E. M. Cabaleiro-Lago and J. Rodríguez-Otero, On the nature of σ–σ, σ–π, and π–π stacking in extended systems, *ACS Omega*, 2018, **3**, 9348–9359.
49 K. Szalewicz, Symmetry-adapted perturbation theory of intermolecular forces, *Wiley Interdiscip. Rev.: Comput. Mol. Sci.*, 2012, **2**, 254–272.
50 E. G. Hohenstein and C. D. Sherrill, Wavefunction methods for noncovalent interactions, *Wiley Interdiscip. Rev.: Comput. Mol. Sci.*, 2012, **2**, 304–326.
51 A. J. Misquitta, *Intermolecular interactions, in Handbook of Computational Chemistry*, ed. J. Leszczynski, Springer Science + Business Media, 2012, ch. 6, pp. 157–193.
52 K. U. Lao and J. M. Herbert, Accurate and efficient quantum chemistry calculations of noncovalent interactions in many-body systems: The XSAPT family of methods, *J. Phys. Chem. A*, 2015, **119**, 235–253.
53 J. M. Herbert, L. D. Jacobson, K. U. Lao and M. A. Rohrdanz, Rapid computation of intermolecular interactions in molecular and ionic clusters: Self-consistent polarization plus symmetry-adapted perturbation theory, *Phys. Chem. Chem. Phys.*, 2012, **14**, 7679–7699.
54 K. U. Lao and J. M. Herbert, Atomic orbital implementation of extended symmetry-adapted perturbation theory (XSAPT) and benchmark calculations for large supramolecular complexes, *J. Chem. Theory Comput.*, 2018, **14**, 2955–2978.
55 K.-Y. Liu, K. Carter-Fenk and J. M. Herbert, Self-consistent charge embedding at very low cost, with application to symmetry-adapted perturbation theory, *J. Chem. Phys.*, 2019, **151**, 031102.
56 M. A. Rohrdanz, K. M. Martins and J. M. Herbert, A long-range-corrected density functional that performs well for both ground-state properties and time-dependent density functional theory excitation energies, including charge-transfer excited states, *J. Chem. Phys.*, 2009, **130**, 054112.
57 K. U. Lao and J. M. Herbert, Symmetry-adapted perturbation theory with Kohn-Sham orbitals using non-empirically tuned, long-range-corrected density functionals, *J. Chem. Phys.*, 2014, **140**, 044108.
58 K. U. Lao and J. M. Herbert, An improved treatment of empirical dispersion and a many-body energy decomposition scheme for the explicit polarization plus symmetry-adapted perturbation theory (XSAPT) method, *J. Chem. Phys.*, 2013, **139**, 034107; Erratum: K. U. Lao and J. M. Herbert, *J. Chem. Phys.*, 2014, **140**, 119901.
59 K. Carter-Fenk, K. U. Lao, K.-Y. Liu and J. M. Herbert, Accurate and efficient *ab initio* calculations for supramolecular complexes: Symmetry-adapted perturbation theory

 This journal is © the Owner Societies 2020

Published on 13 October 2020. Downloaded on 11/11/2020 5:31:14 PM.

with many-body dispersion, *J. Phys. Chem. Lett.*, 2019, **10**, 2706–2714.
60 A. Tkatchenko, R. A. DiStasio Jr., R. Car and M. Scheffler, Accurate and efficient method for many-body van der Waals interactions, *Phys. Rev. Lett.*, 2012, **108**, 236402.
61 R. A. DiStasio, Jr., O. A. von Lilienfeld and A. Tkatchenko, Collective many-body van der Waals interactions in molecular systems, *Proc. Natl. Acad. Sci. U. S. A.*, 2012, **109**, 14791–14795.
62 J. Hermann, R. A. DiStasio Jr. and A. Tkatchenko, First-principles models for van der Waals interactions in molecules and materials: Concepts, theory, and applications, *Chem. Rev.*, 2017, **117**, 4714–4758.
63 J. F. Dobson, Beyond pairwise additivity in London dispersion interactions, *Int. J. Quantum Chem.*, 2014, **114**, 1157–1161.
64 Y. Shao, Z. Gan, E. Epifanovsky, A. T. B. Gilbert, M. Wormit, J. Kussmann, A. W. Lange, A. Behn, J. Deng, X. Feng, D. Ghosh, M. Goldey, P. R. Horn, L. D. Jacobson, I. Kaliman, R. Z. Khaliullin, T. Kús, A. Landau, J. Liu, E. I. Proynov, Y. M. Rhee, R. M. Richard, M. A. Rohrdanz, R. P. Steele, E. J. Sundstrom, H. L. Woodcock III, P. M. Zimmerman, D. Zuev, B. Albrecht, E. Alguire, B. Austin, G. J. O. Beran, Y. A. Bernard, E. Berquist, K. Brandhorst, K. B. Bravaya, S. T. Brown, D. Casanova, C.-M. Chang, Y. Chen, S. H. Chien, K. D. Closser, D. L. Crittenden, M. Diedenhofen, R. A. DiStasio Jr., H. Do, A. D. Dutoi, R. G. Edgar, S. Fatehi, L. Fusti-Molnar, A. Ghysels, A. Golubeva-Zadorozhnaya, J. Gomes, M. W. D. Hanson-Heine, P. H. P. Harbach, A. W. Hauser, E. G. Hohenstein, Z. C. Holden, T.-C. Jagau, H. Ji, B. Kaduk, K. Khistyaev, J. Kim, J. Kim, R. A. King, P. Klunzinger, D. Kosenkov, T. Kowalczyk, C. M. Krauter, K. U. Lao, A. Laurent, K. V. Lawler, S. V. Levchenko, C. Y. Lin, F. Liu, E. Livshits, R. C. Lochan, A. Luenser, P. Manohar, S. F. Manzer, S.-P. Mao, N. Mardirossian, A. V. Marenich, S. A. Maurer, N. J. Mayhall, C. M. Oana, R. Olivares-Amaya, D. P. O'Neill, J. A. Parkhill, T. M. Perrine, R. Peverati, P. A. Pieniazek, A. Prociuk, D. R. Rehn, E. Rosta, N. J. Russ, N. Sergueev, S. M. Sharada, S. Sharma, D. W. Small, A. Sodt, T. Stein, D. Stück, Y.-C. Su, A. J. W. Thom, T. Tsuchimochi, L. Vogt, O. Vydrov, T. Wang, M. A. Watson, J. Wenzel, A. White, C. F. Williams, V. Vanovschi, S. Yeganeh, S. R. Yost, Z.-Q. You, I. Y. Zhang, X. Zhang, Y. Zhao, B. R. Brooks, G. K. L. Chan, D. M. Chipman, C. J. Cramer, W. A. Goddard III, M. S. Gordon, W. J. Hehre, A. Klamt, H. F. Schaefer III, M. W. Schmidt, C. D. Sherrill, D. G. Truhlar, A. Warshel, X. Xu, A. Aspuru-Guzik, R. Baer, A. T. Bell, N. A. Besley, J.-D. Chai, A. Dreuw, B. D. Dunietz, T. R. Furlani, S. R. Gwaltney, C.-P. Hsu, Y. Jung, J. Kong, D. S. Lambrecht, W. Liang, C. Ochsenfeld, V. A. Rassolov, L. V. Slipchenko, J. E. Subotnik, T. Van Voorhis, J. M. Herbert, A. I. Krylov, P. M. W. Gill and M. Head-Gordon, Advances in molecular quantum chemistry contained in the Q-Chem 4 program package, *Mol. Phys.*, 2015, **113**, 184–215.
65 J. P. Perdew, J. Tao, V. N. Staroverov and G. E. Scuseria, Meta-generalized gradient approximation: Explanation of a realistic nonempirical density functional, *J. Chem. Phys.*, 2004, **120**, 6898–6911.
66 F. Weigend and R. Ahlrichs, Balanced basis sets of split valence, triple zeta valence and quadruple zeta valence quality for H to Rn: Design and assessment of accuracy, *Phys. Chem. Chem. Phys.*, 2005, **7**, 3297–3305.
67 F. Neese, F. Wennmohs, U. Becker and C. Riplinger, The ORCA quantum chemistry program package, *J. Chem. Phys.*, 2020, **152**, 224108.
68 T. F. Headen, Temperature dependent structural changes in liquid benzene studied using neutron diffraction, *Mol. Phys.*, 2019, **117**, 3329–3336.
69 K. S. Kim, S. Karthikeyan and N. J. Singh, How different are aromatic π interactions from aliphatic π interactions and non-π stacking interactions?, *J. Chem. Theory Comput.*, 2011, **7**, 3471–3477.
70 M. Gussoni, M. Rui and G. Zerbi, Electronic and relaxation contribution to linear molecular polarizability. An analysis of the experimental values, *J. Mol. Struct.*, 1998, **447**, 163–215.
71 E. G. Hohenstein and C. D. Sherrill, Density fitting and Cholesky decomposition approximations in symmetry-adapted perturbation theory: Implementation and application to probe the nature of π–π interactions in linear acenes, *J. Chem. Phys.*, 2010, **132**, 184111.
72 T. F. Headen, P. L. Cullen, R. Patel, A. Taylor and N. T. Skipper, The structures of liquid pyridine and naphthalene: The effects of heteroatoms and core size on aromatic interactions, *Phys. Chem. Chem. Phys.*, 2018, **20**, 2704–2715.
73 R. L. Brown and S. E. Stein, *Boiling point data, in NIST Chemistry WebBook, NIST Standard Reference Database Number 69*, ed. P. J. Lindstrom and W. G. Mallard, National Institute of Standards and Technology, Gaithersburg, MD, 2020.
74 M.-M. Li, Y.-B. Wang, Y. Zhang and W. Wang, The nature of the noncovalent interactions between benzene and C_{60} fullerene, *J. Phys. Chem. A*, 2016, **120**, 5766–5772.
75 J. P. B. Filipović, M. B. Hall and S. D. Zarić, Stacking interactions of resonance-assisted hydrogen-bridged rings and C_6-aromatic rings, *Phys. Chem. Chem. Phys.*, 2020, **22**, 13721–13728.
76 Y. M. Han, B. Özyilmaz, Y. Zhang and P. Kim, Energy band-gap engineering of graphene nanoribbons, *Phys. Rev. Lett.*, 2007, **98**, 206805.
77 J. O. Sofo, A. S. Chaudhari and G. D. Barber, Graphane: A two-dimensional hydrocarbon, *Phys. Rev. B: Condens. Matter Mater. Phys.*, 2007, **75**, 153401.
78 J. Son, S. Lee, S. J. Kim, B. C. Park, H.-K. Lee, S. Kim, J. H. Kim, B. H. Hong and J. Hong, Hydrogenated monolayer graphene with reversible and tunable wide band gap and its field-effect transistor, *Nat. Commun.*, 2016, **7**, 13261.
79 R. E. Franklin, The structure of graphitic carbon, *Acta Crystallogr.*, 1951, **4**, 253–261.
80 A. Lauchner, A. E. Schlater, A. Manjavacas, Y. Cui, M. J. McClain, G. J. Stec, F. J. García de Abajo, P. Nordlander and N. J. Halas, Molecular plasmonics, *Nano Lett.*, 2015, **15**, 6208–6214.
81 J. Chen, M. Badoili, P. Alonso-González, S. Thongrattanasiri, F. Huth, J. Osmond, M. Spasenović, A. Centeno, A. Pesquera, P. Godignon, A. Z. E. N. Camara, F. J. García de Abajo, R. Hillenbrand and F. H. L. Koppens, Optical nano-imaging of gate-tunable graphene plasmons, *Nature*, 2012, **487**, 77–81.

82 E. H. Hwang and S. D. Sarma, Dielectric function, screening, and plasmons in two-dimensional graphene, *Phys. Rev. B: Condens. Matter Mater. Phys.*, 2007, **75**, 205418.
83 F. H. da Jornada, L. Xian, A. Rubio and S. G. Louie, Universal slow plasmons and giant field enhancement in atomically thin quasi-two-dimensional metals, *Nat. Commun.*, 2020, **11**, 1013.
84 E. R. Johnson, S. Keinan, P. Mori-Sánchez, J. Contreras-García, A. J. Cohen and W. Yang, Revealing noncovalent interactions, *J. Am. Chem. Soc.*, 2010, **132**, 6498–6506.
85 J. Contreras-García, E. R. Johnson, S. Keinan, R. Chaudret, J.-P. Piquemal, D. N. Beratan and W. Yang, NCIPLOT: A program for plotting noncovalent interaction regions, *J. Chem. Theory Comput.*, 2011, **7**, 625–632.
86 N. Ferri, R. A. DiStasio, Jr., A. Ambrosetti, R. Car and A. Tkatchenko, Electronic properties of molecules and surfaces with a self-consistent interatomic van der Waals density functional, *Phys. Rev. Lett.*, 2015, **114**, 176802.
87 A. Sygula and S. Saebø, π–π Stacking of curved carbon networks: The corannulene dimer, *Int. J. Quantum Chem.*, 2009, **109**, 65–72.
88 F. J. Lovas, R. J. McMahon, J.-U. Grabow, M. Schnell, J. Mack, L. T. Scott and R. L. Kuczkowski, Interstellar chemistry: A strategy for detecting polycyclic aromatic hydrocarbons in space, *J. Am. Chem. Soc.*, 2005, **127**, 4345–4349.
89 Ohio Supercomputer Center, http://osc.edu/ark:/19495/f5s1ph73.

Published on 13 October 2020. Downloaded on 11/11/2020 5:31:14 PM.

This journal is © the Owner Societies 2020